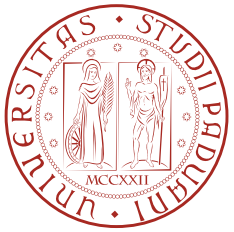

UNIVERSITÀ DEGLI STUDI DI PADOVA

Dipartimento di Fisica e Astronomia "Galileo Galilei"

Corso di Laurea Magistrale in Fisica

Tesi di Laurea

Study of the elastic response of DNA single molecules by means of optical tweezers

Relatore

Dr.ssa Annamaria Zaltron

Correlatore

Prof. Giampaolo Mistura

Laureando

Francesco Raccanello

Anno Accademico 2018/2019

Contents

Introduction

Historically physics and biology aim to describe, characterize and understand the matter (animated or inanimate, using an obsolete nomenclature) starting from its constituent elements. Both sciences built their own set of experimental and theoretical techniques which are usually relegated to own context. Despite of this, in the last 50 years, the knowledge of biology and physics merged tighter in what is called *biophysics*, which aims to investigate biological systems through the methods typical of physics. One example out of many: replication process of DNA which involves complex mechanisms like DNA unwinding, denaturation (the DNA strands are separated by specific protein), formation of the biomolecules and restoring the original molecular conformation. This well-known process can be analyzed in a new light from the physical point of view. As a matter of fact, the energy values typically encountered in such reactions are in the order of few k_BT units and therefore they are strongly affected by energetic fluctuations induced by the presence of the aqueous environment. Statistical thermodynamics, that is a well-established approach for describing complex biological systems, can be useful to investigate this processes. More recently, a new interesting area in biophysics has received great attention from the scientific community, that is the *non-equilibrium thermodynamics of small systems*, which aims to investigate the thermodynamic properties of small system, above all at the single-molecule level[1]. Indeed, the recent technological developments has allowed the transition from bulk experiments (in which the molecular information are derived as average over a number of molecules of the order of Avogadro's number) to *single-molecule experiments* (SME). In this case an individual molecule at a time is investigated and, from its behavior, processes which are usually invisible can be derived.

Nowadays, there are many techniques that can be used to manipulate single molecules, such as Atomic Force Microscopy (AFM) and Magnetic Tweezers, and among them Optical Tweezers (OT) surely merit the attention they heve recently received, thanks to their incredible high spatial (0,2 nm) and time resolution (0,1 ms). Optical tweezers use focused gaussian beams to trap and manipulate biological systems and they can exploit the momentum conservation law to control and monitor the applied forces (from 0,02 pN to 150 pN)

Single-molecule experiments are used to investigate mechanical and thermodynamical properties of many types of biomolecules, such as proteins, molecular motors, RNA and DNA and this thesis fits into this context. In particular, in this thesis work the elastic response of double-stranded DNA molecules are investigated by means of high-frequency force spectroscopy with optical tweezers. Understanding the DNA elasticity properties is

the cornerstone for a better comprehension of its biological properties and functionalities. Nowadays three main questions are still under debate, that are the behavior of the DNA when it is subject to a force around 67 pN, in the so called over-stretching regime, its elastic response above this range and the role played by the coupling of the stretch and twist of the molecule. In particular this last aspect has been recently investigated by means of molecular dynamics simulations[2] and magnetic tweezers[3, 4], but these results partially contradict previous investigations and a clear and widely-accepted theoretical model explaining this effect is still lacking. Therefore the main goal of this thesis was the demonstration of the feasibility of a new experimental approach for shedding light on some unsolved problems on DNA elastic behavior.

The experimental protocol uses DNA molecules tethered between two beads that are trapped by a costume made micro-pipette and the optical tweezer laser beam. By moving the position of the trap, the DNA is elongated and the force exerted is recorded by the high sample rate acquisition system. The experiments take place in a fluidic chamber which has been optimized in order to have the optimum set-up conditions. As a metter of fact, and any misalignment or leaks in the fluidic chamber can compromise the data acquisition.

The first step was the calibration and the characterization of the apparatus and then the experimental protocol was optimized by tuning the dilution ratio used for beads incubation, a procedure in which the DNA is directly bond to one of the two beads.

The acquired data were analyzed transforming the raw voltage signal of the electronic board into the force spectrum signal and this was interpolated with a lorentzian curve in order to extract its amplitude and the corner frequency. These parameters were correlated to the elastic parameters of the DNA by means of a theoretical model and the role played by the size of the DNA was investigated by performing the experiments on molecules with different lengths.

The thesis is so organized:

Chapter 1: In the first chapter the physical principles of the optical tweezer and the theory of the direct force measurement will be presented.

Chapter 2: In the second chapter the optical tweezer set-up, the calibration procedure and the preliminary steps of the experimental protocols will be described

Chapter 3: In the third chapter some basic notions about the DNA structure will be presented, then the DNA molecules used in this work will be introduced, and finally the theoretical models that describe the elastic properties of DNA will be discussed.

Chapter 4: In the last chapter the results obtained through the experimental protocol will be presented and discussed.

Chapter 1

Physical principle of optical tweezer

The underlying physical theory of optical trap is based on the interaction of mesoscopic particles and the electromagnetic field, which, as is known from the theory, carries momentum and energy.

Although the first hypotheses[5] about the existence of radiation pressure were known already in the sixteenth century with Kepler and in the seventeenth with Newton and Euler, who were interested in the study of the tail of comets, and corroborated by experimental observations such as Crookes radiometer (1873), the general theory of the phenomenon found its general theoretical framework in Maxwell's 1865 treatise on the dynamic theory of the electromagnetic field, which formalizes classical electromagnetism. An independent explanation of the movement produced by light and heat through a thermodynamic approach was provided, independently, also by the Italian Bartoli [6] (1876).

The interaction between electromagnetic waves and matter was studied by Lorenz[7, 8] which, using a mechanical approach, found a equivalent description to the Mie's rigorous electromagnetic approach for plane waves scattered by a sphere[9, 10]. The theory was tackled by Debye[11] who discussed the force due to radiation pressure. This theory, called[12] Lorenz-Mie theory (LMT), describes the interaction between a plane electromagnetic wave propagating in a homogeneous and non-absorbent medium, with a homogeneous spherical particle characterized by its radius and refractive index. With the rise of laser, in the 1960 by Maiman, began the first applications of this technology for characterization experiments, such as the estimation of the velocity of a liquid via the tracking of particles transported by the flow[13] or simultaneous measurement of velocity and size of spherical particles in certain multiphase flows[14]. From these first studies emerged the limits of the theory of Lorenz-Mie when the transversal dimension of the laser beam was comparable with that of the interacting particle. Therefore it was necessary to extend the theory in what is nowadays called Generalized Lorenz-Mie theory (GLMT)[15].

The first studies on the mechanical effect of laser light on particles were made by Arthur Ashkin, awarded of the Nobel Prize in 2018, together with the physicists Donna Strickland and Gérard Mourou in the field of lasers, "for optical tweezers and their application to biological systems". In a first article in 1970[16] was described the interaction of a semitransparent spherical ball (radius $a = 2{,}68\,\mu\text{m}$) with a focused laser beam of a few milliwatts ($\lambda = 514{,}5\,\text{nm}$, TEM_{00} mode and waist $w_0 = 6{,}2\,\mu\text{m}$) observing that

when the particle moved away from the optical axis, it experienced both a force which attracted it towards the region of higher light intensity (that is the center of the laser beam) and a force which pushed the particle along the propagation direction of the beam (already known as pressure force, or scattering force). A first theoretical treatment of the phenomenon uses a geometric optics approach. The laser beam is decomposed into light rays which are reflected and refracted, thus determining the forces responsible for the observed phenomenon. Considering the refractive index of the particle greater than the one of the medium, that is when the relative refractive index $m = n_p/n_m > 1$, it is possible to consider the sphere as a converging lens which determines the acceleration of the particle towards the region of highest intensity of the beam and in the direction of its propagation. It is predicted, and confirmed experimentally by observing air bubbles of diameter 8 µm in a high viscosity medium, that by swapping the magnitude of refractive indices, the spherical particle behaves like a divergent lens, reversing the direction of the radial forces and driving the particle away from the optical axis. To cancel the transverse force in the direction of the beam a second laser, identical to the first except for the counterpropagating direction, is introduced allowing thus to obtain an optical potential well or "optical bottle". Subsequent studies[17–19] considered the levitation of small transparent spheres in air and vacuum ($\sim 7\,\text{Torr}$ and $\sim 10^{-6}\,\text{Torr}$) investigating their stability. In 1986[20] Ashkin et al. reported the experimental evidence on the possibility of *trapping with a single ray* a particle of size from 10 µm to 25 nm. Appears, for the first time, the distinction between scattering force (the one in the beam direction proportional to the light intensity) and gradient force (directed towards the region of maximum beam intensity, which is dependent on the gradient of the light intensity), an the observation that the latter, for a strongly focused beam, has an axial component that dominates the former, thus making the trap more stable. In 1992[21] was published the analysis, again under hypotheses of geometric optics regime, where scattering and gradient forces were provided depending on the position of the spherical particle in relation to the laser fire. The effects of the mode TEM_{00} and TEM^*_{00} as well as the role of the refractive index were analyzed. For the first time the laser trap of a single beam was defined as "optical tweezers". Further work of Ashkin focused on the use of radiation pressure on non-ionized atoms, and in 1987 he studied the application of optical tweezers in biological systems for the manipulation of bacteria and viruses in aqueous solutions[22], both with visible argon laser light and infrared systems to reduce the optical damage of systems such as cellular ones.

1.1 Theoretical models of optical trapping

From the theoretical point of view, the interaction of the electromagnetic field with the dielectric particle can be approached using three models depending on the ratio between the diameter of the sphere and the wavelength of the radiation used. In all cases, the system under investigation is well described by classical physics, except the description the optical beam as a photons flow.

Mie regime or geometrical optics When the size of the dielectric particle, i.e. its diameter $2a$, is greater than the wavelength λ of the light used, $2a \gg \lambda$, it's possible

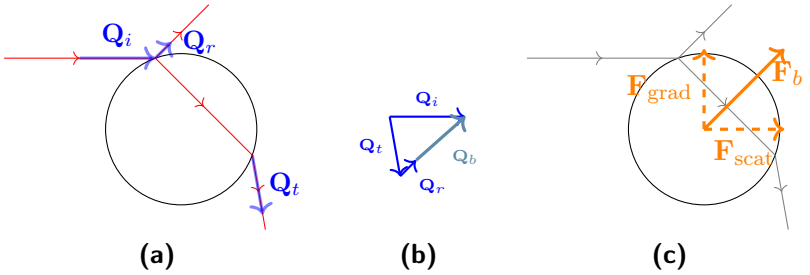

Figure 1.1
Interaction of a homogeneous beam with a spherical particle, whose radius is much greater than the wavelength from the light source (mode of Mie or geometric optics). The variation of the momentum (b) gives origin to a force (c) that can be decomposed in the parallel and same direction and equals the beam and the orthogonal component.

neglect undulatory aspects of light and apply the principles of the geometrical optics regime, also called Mie regime.[21, 23–25]

The assumptions of this model consider the optical beam as the composition of light rays each of them characterized by certain light intensity, polarization and traveling in a straight line in a homogeneous medium. In accordance with Fresnel's theory, the interaction with an interface can change the direction of the beam by reflection or refraction, as also its polarization. In this model it is possible to ignore diffraction phenomena. The beads, made of dielectric material, is considered transparent with a real refractive index (there are no complex terms that would describe the absorption of light) making only reflection or refraction possible. The simplest model that can be introduced to explain the nature of scattering and gradient forces, considers a uniform beam of light which interacts with a transparent bead by partially transferring its linear momentum (see Figure 1.1). Said $\mathbf{Q}_i$, $\mathbf{Q}_r$, $\mathbf{Q}_t$ e $\mathbf{Q}_b$ the linear momentum carried by the incident ray, the reflected and refraction ones and that of the bead, respectively, the law of the conservation of momentum states that:

$$\mathbf{Q}_i = \mathbf{Q}_r + \mathbf{Q}_t + \mathbf{Q}_b$$

or that the momentum transferred to the particle is equal to:

$$\mathbf{Q}_b = \mathbf{Q}_i - (\mathbf{Q}_r + \mathbf{Q}_t)$$

from which the force experienced by the particle is derived:

$$\mathbf{F}_b = \frac{\mathrm{d}\mathbf{Q}_b}{\mathrm{d}t}$$

Usually the light intensity of the reflected ray is much more feeble than the refracted ray and therefore, with good approximation, the force is given by the difference between the linear momenta of the incident and refracted light. The vector obtained can be decomposed along the propagation direction of the incident beam and along the orthogonal component. The first is called *scattering force* or axial force, while the second is defined

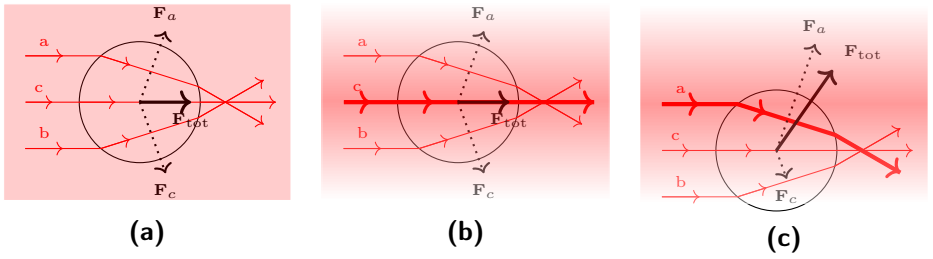

Figure 1.2
The interaction of a homogeneous light beam, (a), and beam with gaussian profile, (b) and (c), with a spherical particle having a radius much greater than the wavelength from the light source (Mie regime or geometrical optics). In the first case the total force acting on the particle is only in the direction of propagation of the beam; in the case of a gradient of intensity, a term of force that lead the center of the sphere to coincide with the beam optical axis.

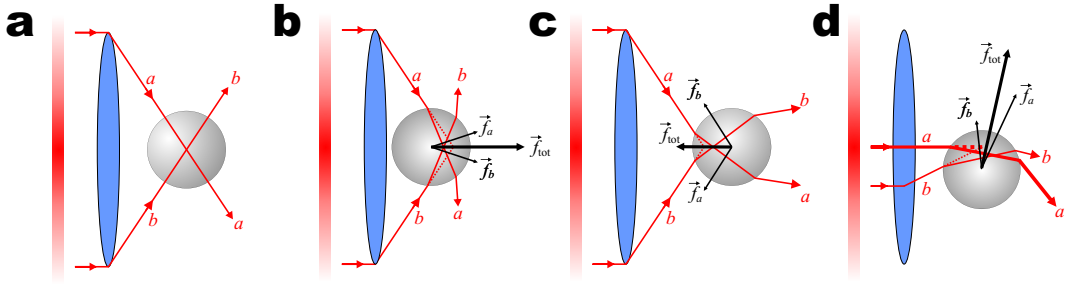

Figure 1.3
By focusing a beam it is possible to obtain an overall pull force that tends to trap the sphere at the focus of the lens.

as *gradient force* or radial force. The sum of the forces originating from all rays determines the total force acting on the bead. As shown in Figure 1.2a, in the case of a uniform beam of light, the symmetry of the system makes the non-axial components of the force to cancel each other out, so that the total final force is the scattering one, which is oriented along the propagation direction of the laser beam. Even in the case of collimated Gaussian beam which presents a non-zero gradient force, the scattering force is usually dominant, so that the particle is still pushed along the light propagation direction and a stable confinement is not achieved. In the case of single collimated beams, therefore, the optical trapping could not be realized.

Focusing the beam (see Figure 1.3), however, it is possible to obtain a total force directed from the center of the particle to the focus of the beam itself, thus giving rise to a pull force that tends to align the two points and obtaining the trapping phenomenon.

Considering a beam focused in a geometric point through a high numerical aperture lens (e.g. $NA = 1{,}25$), it is possible to determine the force due to the variation of the momentum of a reflected and refracted ray. Let be P the beam power when it reaches the interface of the sphere, forming an angle θ from the normal at the intersection point. When the beam is reflected and refracted by the sphere, according to the usual laws of geometric optics, the power will vary according to the Fresnel's coefficients of reflection

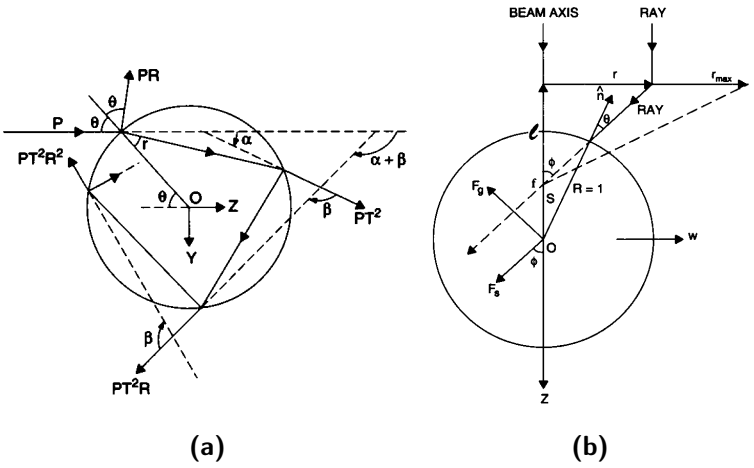

Figure 1.4
In (a) it is shown the analysis of the reflection and refraction of an incident beam on a semi-transparent particle. The power P is distributed according to the reflection R and transmission T coefficients. In (b) the force acting on the bead is decomposable into scattering and gradient components.

R and transmission T. When the beam is first reflected, its power will be PR, while when the beam is transmitted, emerging from the beads and propagating forward into the medium, it will have a power of PT^2 (because undergone into two refractions: medium - beads, beads - medium). In general, the power of a ray that exits the particle after n reflection will be PT^2R^n, and it will form an angle of $\alpha + n\beta$ with the incident beam direction, as can be seen form Figure 1.4. The force can be derived as the light momentum variation over time and it can be decomposed into two perpendicular components, one parallel to the beam propagation direction, F_z, and the other perpendicular to it, F_y, thus obtaining:

$$F_z = \frac{n_p P}{c} - \left[\frac{n_p PR}{c}\cos(\pi + 2\theta) + \sum_{n=0}^{\infty}\frac{n_p P}{c}T^2R^n\cos(\alpha + n\beta)\right]$$
$$F_y = 0 - \left[\frac{n_p PR}{c}\sin(\pi + 2\theta) + \sum_{n=0}^{\infty}\frac{n_p P}{c}T^2R^n\sin(\alpha + n\beta)\right]$$

If the problem is considered in the complex plane, and introducing the total force defined as:

$$F_{tot} = F_z + iF_y$$

so it can be write the total force as:

$$F_{tot} = \frac{n_p P}{c}[1 + R\cos 2\theta] + i\frac{n_p P}{c}R\sin(2\theta) - \frac{n_p P}{c}T^2\sum_{n=0}^{\infty}R^n e^{i(\alpha+n\beta)}$$

obtaining, thus, a geometric series[1] in the last term, whose results, as known, provides:

$$F_{tot} = \frac{n_p P}{c}[1 + R\cos 2\theta] + i\frac{n_p P}{c}R\sin(2\theta) - \frac{n_p P}{c}T^2 e^{i\alpha}\left[\frac{1}{1 - Re^{i\beta}}\right]$$

Rationalizing the denominator of the last addends and taking the real and complex part, scattering and gradient forces could be obtained:

$$F_z = F_{\text{scattering}} = \frac{n_p P}{c}\left\{1 + R\cos 2\theta - \frac{T^2[\cos(2\theta - 2r) + R\cos 2\theta]}{1 + R^2 + 2R\cos 2r}\right\} \tag{1.1}$$

$$F_z = F_{\text{gradient}} = \frac{n_p P}{c}\left\{R\sin 2\theta - \frac{T^2[\sin(2\theta - 2r) + R\sin 2\theta]}{1 + R^2 + 2R\cos 2r}\right\} \tag{1.2}$$

where θ and r are incident and refractive angles respect to the optical axis.

This results are exact because no truncation has been performed in the terms of the series; the dependence on the Fresnel coefficients R and T inherit the dependence on the type of light polarization.

The proposed approach is also applicable to beams with complex geometries, such as the strongly focused Gaussian one. Looking at Figure 1.5 it reports numerical simulations[21] showing how the force experienced by the particle changes when this latter moves from the center of the focused gaussian beam. In general, the total force is assumed to be proportional to the dimensionless parameter Q_t, whose components Q_s and Q_g refers to the scattering and gradient force, respectively. As highlighted in Figure 1.5b, the parameter Q_s becomes relevant when the particle moves away from the focal point of the focused beam. Moreover (ree Figure 1.5d), the parameter Q_g dominates on Q_s when the particle is not perfectly align with the optical axis of the gaussian beam.

It can be shown that gradient force is conservative despite of scattering force whose work is path dependent; this result will be more evident in the Rayleigh regime. Finally, for Mie's regime, the forces have no dependence on the size of the sphere (i.e. $\mathbf{F} \propto a^0$). Although the validity of this approach requires that $2a \gg \lambda$, the comparison between experimental measurements and numerical simulations confirmed the validity of this approach within the limit of $2a/\lambda \geq 7$.[26]

Rayleigh regime When the condition required by the Mie regime is no longer valid, but vice versa it's observe $2a \ll \lambda$, the wave nature of light and the interaction of the electromagnetic field with matter must be taken into account in order to obtain a model suitable for experimental observations. This is the so-called Rayleigh regime[23, 24, 27]. In the following the particle will be considered point-like and immersed in an electromagnetic field variable in time. The electric field inside the particle is uniform, while instantly the electric field around the particle remains unchanged and causes its polarization by inducing an electric dipole. Under these assumptions the problem is similar to the electrostatic case.

The time variation of the electromagnetic field produces a synchronous vibration of the dipole of the particle which then produces scattering waves around it. This gives rise

[1] Due to energy conservation, $Re^{i\beta}$ will be always positive value and less than the unit.

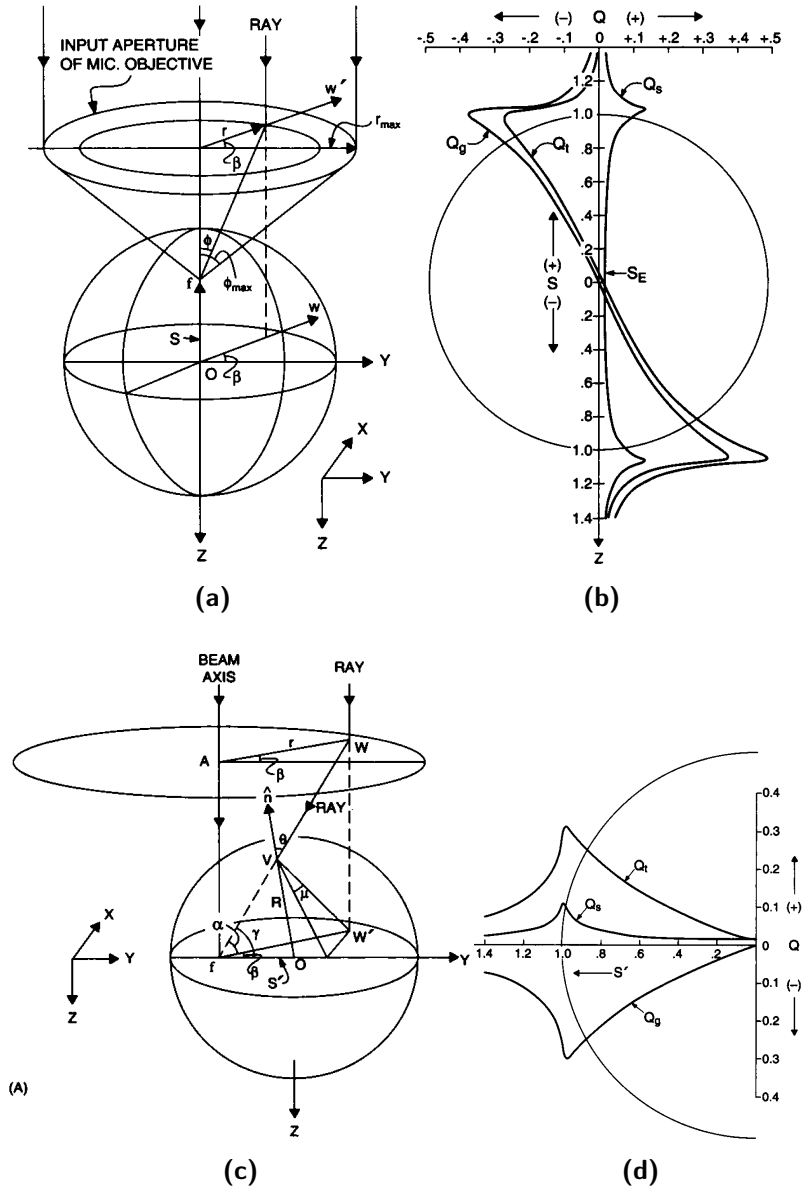

Figure 1.5
In (a) it is illustrated the interaction between a focused beam and a sphere aligned with the optical axis, whose center deviates by an amount equal to S from the center from the focal point. In (b) there are numerical estimates of the dimensionless term Q defined from the force: $F = Qn_pP/c$: Q_s indicates the one relative to the scattering force, Q_g for gradient force and Q_t for total force. Although the term scattering is positive, the term gradient, which is antisymmetric, is dominant. The total force, thus, has a minimum near $S \simeq 0$, that is when the center of the sphere is next to the fire. In (c) and (d) the same amounts are reported in case the center of the sphere is outside the optical axis in the $\hat{y}$ direction. Again the total force presents a minimum when the center of the sphere is close to the position of the fire.
Source: Ashkin [21]

to deviations in the direction of the incident field with the consequent transfer of momentum from the incident wave to the induced dipole. From this variation the scattering force is originated and it can be calculated as:

$$\mathbf{F}_{scattering}(\mathbf{r}) = \left(\frac{n_m}{c}\right)\sigma_{pr} I(r)\hat{\mathbf{z}}$$

where n_m is the refraction index of the medium, σ_{pr} is the cross section between the particle and the radiation, while $\hat{\mathbf{z}}$ is the unit vector of the propagation direction of the light. For a spherical body, of radius a the cross section is:

$$\sigma_{pr} = \frac{128\pi^5 a^6}{3\lambda^4}\left(\frac{m^2-1}{m^2+2}\right)^2$$

where m is the relative refractive index of the particles and is given by the ratio of the refractive index of the particle to that of the medium: $m = n_p/n_m$.

$$\mathbf{F}_{scattering}(\mathbf{r}) = \left(\frac{n_m}{c}\right)\frac{128\pi^5}{3\lambda^4}a^6\left(\frac{m^2-1}{m^2+2}\right)^2 I(r)\hat{\mathbf{z}} \tag{1.3}$$

As it is possible to notice, the scattering force changes according to the intensity profile of the incident beam and therefore it is more intense in corrispondence fo the optical axus of the beam, where the light intensity is higher.

The electric dipole of the particle interacts with the electric field also by the force of Lorentz. Given a dipole $\mathbf{p}(\mathbf{r},t)$ the force is derived by $\mathbf{F} = -\nabla U = \nabla[\mathbf{p}(\mathbf{r},t)\cdot\mathbf{E}(\mathbf{r},t)]$ where the electric dipole moment induced on the particle is given by:

$$\mathbf{p}(\mathbf{r},t) = 4\pi n_m^2 \epsilon_0 a^3\left(\frac{m^2-1}{m^2+2}\right)\mathbf{E}(\mathbf{r},t)$$

from which, taking the temporal average of the force, is obtained:

$$\mathbf{F}_{\text{gradient}}(\mathbf{r},t) = \frac{2\pi n_m}{c}a^3\left(\frac{m^2-1}{m^2+2}\right)\nabla I(r) \tag{1.4}$$

Since the gradient force attracts the particle towards the center of the beam, this force can be also rewritten as an elastic force due to the interaction of the trapped particle with an harmonic potential. In the following it will be assumed that the beam has a Gaussian radial profile, whose intensity is therefore given by:

$$I(r) \simeq I_0 e^{-\frac{2r^2}{w_0^2}}$$

where I_0 is maximum intensity of the light beam and w_0 is the diameter of the beam. By replacing the above formula in equation (1.4), and approximating the exponential by small deviations from the equilibrium point, it is found that the force can be rewritten as:

$$\mathbf{F}_{\text{gradient}}(\mathbf{r}) = -k\mathbf{r} \tag{1.5}$$

$$k = \frac{2\pi n_m}{c}a^3\left(\frac{m^2-1}{m^2+2}\right)\frac{I_0}{w_0^2} \tag{1.6}$$

where k is the stiffness of the optical trap. The equation (1.5) will be useful in the following and will be considered as the total force acting on a trapped particle: this is justified by the experimental use of two counter-propagating beams that allow to cancel the scattering force thus improving the optical trap.

The scattering and gradient forces naturally emerge from the study of the interaction between the electromagnetic field and the dipole induced in the illuminated particle. The first of these two has the same direction of the beam and is proportional to its intensity and the sixth power of the radius of the particle; while the conservative gradient force is directed to the higher brightness position in systems where $n_p > n_m$ and is proportional to the third particle radius power of $\mathbf{F} \propto a^3$.

Although most experiments with biological systems are not within the Rayleigh regime, this model together with the previous one provide the two theoretical endpoints. The intermediate region needs a generalization of the theory of Lorenz-Mie.

Generalized Lorenz-Mie Theory regime In the Lorenz-Mie's theory the scattering of a plane wave is analyzed for a homogeneous sphere; however, when the dimension of the beam is comparable with the particle, or for arbitrary beam geometry and positions a generalization of the theory is required[15].

Using Maxwell's theory, it is possible to study the interaction between a dielectric medium and a variable electromagnetic field. As known, in presence of electric charges in an electromagnetic field, the Lorentz's force is:

$$\mathbf{F} = q[\mathbf{E} + \mathbf{v} \times \mathbf{B}]$$

that can be expressed as temporal evolution of the linear momentum of the particle$\mathbf{Q}_p$:

$$\mathbf{F} = \frac{\mathrm{d}\mathbf{Q}_p}{\mathrm{d}t} = q[\mathbf{E} + \mathbf{v} \times \mathbf{B}]$$

From the energetic point of view, it could be useful to write the time variation of kinetic energy of the particle:

$$\frac{\mathrm{d}E_k}{\mathrm{d}t} = m\mathbf{v} \cdot \frac{\mathrm{d}\mathbf{v}}{\mathrm{d}t} = \mathbf{v} \cdot \frac{\mathrm{d}\mathbf{q}_p}{\mathrm{d}t} = q\mathbf{E} \cdot \mathbf{v}$$

Considering the Maxwell equations, depending on the macroscopic charges and current ρ_f and $\mathbf{J}_c$:

$$\nabla \cdot \mathbf{D} = \rho_l \tag{1.7}$$

$$\nabla \times \mathbf{E} = -\frac{\partial \mathbf{B}}{\partial \mathbf{t}} \tag{1.8}$$

$$\nabla \cdot \mathbf{B} = 0 \tag{1.9}$$

$$\nabla \times \mathbf{H} = \mathbf{J}_c + \frac{\partial \mathbf{D}}{\partial t} \tag{1.10}$$

where $\mathbf{E}$ is the electric field, $\mathbf{B}$ is magnetic induction field, $\mathbf{D}$ electric displacement vector,

H is the magnetic filed vector, respectively defined[2] as:

$$\mathbf{D} = \epsilon_0 \mathbf{E} + \mathbf{P}$$
$$\mathbf{H} = \frac{\mathbf{B}}{\mu_0} - \mathbf{M}$$

where **P** is electric polarization and **M** the magnetization. Shall be considered moreover, the constitutive relationships, whose nature is not universal but which are useful for the description of *linear*, *homogeneous* and *isotropic* medium as those considered:

$$\mathbf{J}_c = \sigma \mathbf{E}$$
$$\mathbf{B} = \mu \mathbf{H}$$
$$\mathbf{P} = \epsilon_0 \chi \mathbf{E}$$

where σ is the electric conductivity, μ the magnetic permeability and χ the susceptibility.

For a system presenting a continuous charge distribution of density ρ and electric current density $\mathbf{J} = \rho \mathbf{v}$, the previous equations become:

$$\frac{\partial \mathbf{q}_p}{\partial t} = \rho \mathbf{E} + \mathbf{J} \times \mathbf{B}$$
$$\frac{\partial w_p}{\partial t} = \mathbf{J} \cdot \mathbf{E}$$

where q_p and w_p are the momentum and kinetic energy density respectively. With this equations the correlation between the variation of momentum and kinetic energy and the the electromagnetic field is explicit.

Takin into account the vectorial identity:

$$\nabla \cdot (\mathbf{E} \times \mathbf{H}) = -\mathbf{E} \cdot \nabla \times \mathbf{H} + \mathbf{H} \cdot \nabla \times \mathbf{E}$$

and by replacing the curls with the terms given by the Maxwell equation, the following relation are derived:

$$\begin{aligned} \nabla \cdot (\mathbf{E} \times \mathbf{H}) &= -\mathbf{E} \cdot \left(\mathbf{J}_c + \frac{\partial \mathbf{D}}{\partial t} \right) + \mathbf{H} \cdot \left(-\frac{\partial \mathbf{B}}{\partial \mathbf{t}} \right) \\ &= -\mathbf{J} \cdot \mathbf{E} - \frac{\partial}{\partial t} \left(\frac{1}{2} \mathbf{E} \cdot \mathbf{D} + \frac{1}{2} \mathbf{H} \cdot \mathbf{B} \right) \\ \nabla \cdot \mathbf{S} &= -\frac{\partial w_p}{\partial t} - \frac{\partial}{\partial t} w_f \end{aligned}$$

where the energy density of the field, w_f, and the Poynting's vector **S** were introduced. The equation of continuity is thus derived:

$$\nabla \cdot \mathbf{S} = -\frac{\partial}{\partial t}(w_p + w_f) \tag{1.11}$$

$$\int\limits_{\Sigma = \partial V} \mathbf{S} \cdot \hat{\mathbf{n}} \, \mathrm{d}\Sigma = -\frac{\partial}{\partial t} \int\limits_{V} (w_p + w_f) \, \mathrm{d}V \tag{1.12}$$

[2] In the definition of **D** it is assumed that quadrupole moment and higher orders are negligible.

where the second equation, obtained from Gauss' theorem, expresses energy conservation: the power flow coming out of a closed surface Σ, which encloses a volume V, is equal to the energy decreasing of the system composed by the particle and the field in the volume V.

An analogous equation can be derived for the flow of the momentum. As a matter of fact, by considering the time variation of the Poynting's vector, and replacing the terms present in Maxwell's equations:

$$\frac{\partial \mathbf{S}}{\partial t} = \frac{\partial}{\partial t}(\mathbf{E}\times\mathbf{H}) = \frac{\partial \mathbf{E}}{\partial t}\times\mathbf{H} + \mathbf{E}\times\frac{\partial \mathbf{H}}{\partial t}$$

$$\mu_0\epsilon_0\frac{\partial \mathbf{S}}{\partial t} + \mathbf{J}\times\mathbf{B} = \mu_0(\nabla\times\mathbf{H})\times\mathbf{H} + \epsilon_0(\nabla\times\mathbf{E})\times\mathbf{E}$$

$$\mu_0\epsilon_0\frac{\partial \mathbf{S}}{\partial t} + \mathbf{J}\times\mathbf{B} = \epsilon_0\left[(\mathbf{E}\cdot\nabla)\mathbf{E} - \frac{1}{2}\nabla^2\mathbf{E}^2\right] + \mu_0\left[(\mathbf{H}\cdot\nabla)\mathbf{H} - \frac{1}{2}\nabla^2\mathbf{H}^2\right]$$

$$\begin{aligned}\mu_0\epsilon_0\frac{\partial \mathbf{S}}{\partial t} + \mathbf{J}\times\mathbf{B} + \epsilon_0\mathbf{E}(\nabla\cdot\mathbf{E}) + \mu_0\mathbf{H}(\nabla\cdot\mathbf{H}) = \\ -\frac{1}{2}\nabla[\epsilon_0E^2 + \mu_0H^2] + \epsilon_0[(\mathbf{E}\cdot\nabla)\mathbf{E} + \mathbf{E}(\mathbf{E}\cdot\nabla)] \\ + \mu_0[(\mathbf{H}\cdot\nabla)\mathbf{H} + \mathbf{H}(\mathbf{H}\cdot\nabla)]\end{aligned}$$

it could be obtained the formula, using dyadic notation:

$$\frac{\partial}{\partial t}(\mu_0\epsilon_0\mathbf{S} + \mathbf{q}_p) = -\nabla\left[\left(\frac{1}{2}\epsilon_0E^2 + \frac{1}{2}\mu_0H^2\right)\mathbb{1} - \epsilon_0\mathbf{E}\mathbf{E} - \mu_0\mathbf{H}\mathbf{H}\right]$$

To simplify the previous formulae it is useful to introduce the Maxwell stress tensor $\mathbf{T}$, which represents the flux of the linear momentum of the electromagnetic field and the linear momentum density of the electromagnetic field $\mathbf{q}$ that are defined as:

$$\begin{aligned}\mathbf{T} &= -\left(\frac{1}{2}\epsilon_0E^2 + \frac{1}{2}\mu_0H^2\right)\mathbb{1} - \epsilon_0\mathbf{E}\mathbf{E} - \mu_0\mathbf{H}\mathbf{H} \\ T_{ij} &= -\frac{1}{2}\delta_{ij}(\epsilon_0E^2 + \mu_0H^2) + \epsilon_0E_iE_j + \mu_0H_iH_j\end{aligned} \tag{1.13}$$

$$\mathbf{q}_f = \epsilon_0\mu_0\mathbf{S} \tag{1.14}$$

could be get the linear momentum conservation equation:

$$\nabla\cdot\mathbf{T} = \frac{\partial}{\partial t}(\mathbf{q}_p + \mathbf{q}_f) \tag{1.15}$$

$$\int_{\Sigma=\partial V}\mathbf{T}\cdot\hat{\mathbf{n}}\,\mathrm{d}S = \frac{\partial}{\partial t}\int_V(\mathbf{q}_p + \mathbf{q}_f)\,\mathrm{d}V \tag{1.16}$$

The left-hand side of the equation, describes the total momentum change in the volume V limited by the surface S, while the right-hand side is the force density acting on the surface and depends solely on the electromagnetic field.

$$\mathbf{F} = \int_V\nabla\cdot T = \int_{\Sigma=\partial V}T\cdot\hat{\mathbf{n}}\,\mathrm{d}S \tag{1.17}$$

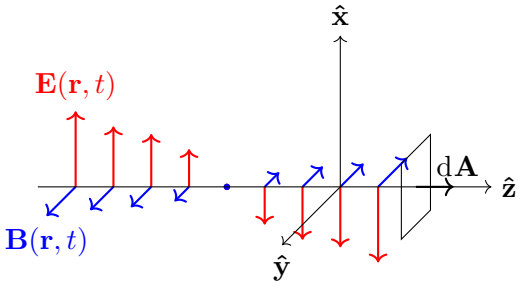

Figure 1.6
Schematic representation of electromagnetic field propagating in the $\hat{\mathbf{z}}$ direction.

On the basis of these results, the GLMT theory describes the interaction between an arbitrary light beam and a dielectric particle.

From these general considerations it will be possible to derive the force acting on the sphere starting from the variation of intensity and the position of the light emitted by the particle on a detector.

1.2 Theory of the direct force measurement

The equation (1.16) generalizes the conservation of the momentum in non-insulated systems and in particular allows to determine the force acting on on a trapped particle based on the variation over time of the momentum of the electromagnetic field and its stress tensor flux:

$$\mathbf{F}_p = \frac{\partial}{\partial t}\int_V \mathbf{q}_p \,\mathrm{d}V = \int_{\Sigma=\partial V} \mathbf{T}\cdot\hat{\mathbf{n}}\,\mathrm{d}S - \frac{\partial}{\partial t}\int_V \mathbf{q}_f \,\mathrm{d}V$$

In particular, in the stationary field hypothesis the last term in the second member vanish and the force calculation on the particle is reduced to the estimate of the momentum flux through a surface S:

$$\mathbf{F}_p = \int_{\Sigma=\partial V} \mathbf{T}\cdot\hat{\mathbf{n}}\,\mathrm{d}S$$

With this in mind, it is evident that a direct measurement of the trapping force could be made possible by the use of optical sensors able to monitor any change in the flux of linear momentum of the light beam, due to its interaction with a trapped object. This goal is more easily achieved when a plane wave linearly polarized is used as light source. As a matter of fact, in this case the Maxwell stress tensor T_{ij} in the last formula could be replaced by the Poyinting vector $\mathbf{S}$ and, in practice, the estimation of the force would not require to directly calculate the Maxwell stress tensor but only its flux through the intensity of the scattered light, as explained in details in the following.[24, 28].

Considering a plane and linearly polarized electromagnetic wave:

$$\mathbf{E}(\mathbf{r},t) = E_x(z,t)\,\hat{\mathbf{x}} = E_0 e^{i(\omega t - kz)}\,\hat{\mathbf{x}}$$
$$\mathbf{B}(\mathbf{r},t) = B_y(z,t)\,\hat{\mathbf{y}} = B_0 e^{i(\omega t - kz)}\,\hat{\mathbf{y}}$$

the electromagnetic stress tensor (1.13) is reduced in the form:

$$\mathbf{T} = \begin{pmatrix} -\frac{\epsilon_0}{2}E_x^2 + \frac{1}{2\mu_0}B_y^2 & & \\ & +\frac{\epsilon_0}{2}E_x^2 - \frac{1}{2\mu_0}B_y^2 & \\ & & -\frac{\epsilon_0}{2}E_x^2 - \frac{1}{2\mu_0}B_y^2 \end{pmatrix}$$

which can be further simplified by recalling the relation $E_0 = cB_0$:

$$\mathbf{T} = \begin{pmatrix} 0 & 0 & 0 \\ 0 & 0 & 0 \\ 0 & 0 & -\epsilon_0 E_x^2 \end{pmatrix}$$

Considered a surface element, $\mathrm{d}A$ of the particle, along $\hat{\mathbf{z}}$ direction (see Figure 1.6) the force will be expressed as:

$$\mathrm{d}\mathbf{F}_p = \mathbf{T} \cdot \hat{\mathbf{n}}\, \mathrm{d}A = -\epsilon_0 E_x\, \mathrm{d}A\, \hat{\mathbf{z}}$$

Using the Poynting vector definition:

$$\mathbf{S} = \mathbf{E} \times \mathbf{H} = -c\epsilon_0 E_x\, \hat{\mathbf{z}}$$

the force assumes the forms:

$$\mathrm{d}\mathbf{F}_p = \frac{n_m}{c}\, \mathbf{S}\, \mathrm{d}A$$

where the refractive index n_m of the medium in which light propagated has been taken into account. This result is valid only when the propagating direction of the electromagnetic field is orthogonal to the surface S. Experimentally this condition can be achieved by requiring the incident ray to be a focused spherical wave. It will be assumed that the emitted ray is radiate as spherical wave from a point, i.e the particle, supposed to be coincident with the focus of the focalizing lens.

By introducing the angular intensity distribution for light, $\mathscr{I}(\theta_m, \phi)$, where θ_m and ϕ are the angles indicated in Figure 1.7:

$$\mathscr{I}(\theta_m, \phi)\hat{\mathbf{r}}\, \mathrm{d}\Omega = \mathbf{S}\, \mathrm{d}A$$

with $\mathrm{d}\Omega = \mathrm{d}A/R^2$ the solid angle element, the force felt by the particle can be written as:

$$\mathbf{F}_p = \frac{n_m}{c} \int_S \mathscr{I}(\theta_m, \phi)(\hat{\mathbf{x}} \sin\theta_m \cos\phi + \hat{\mathbf{y}} \sin\theta_m \sin\phi + \hat{\mathbf{z}} \cos\theta_m)\, \mathrm{d}\Omega \tag{1.18}$$

By convention, it is assumed that the value of $\mathscr{I}(\theta_m, \phi)$ is positive for a ray leaving the system, while it is negative for an incoming one; furthermore, if there is no particle deflecting the beam $\mathscr{I}(\theta_m, \phi) = -\mathscr{I}(-\theta_m, -\phi)$ and the integral vanish, as expected.

Although it remains a complicated problem to predict the value of $\mathscr{I}(\theta_m, \phi)$, it is not complex to *measure it*. The Abbe's sine condition states that a ray emanating from the main focus of a lens, free of comatic aberrations, inclined by an angle θ_m from the optical axis, but that still intercepts the lens, will exit from the main plane from the part of the image with a radial distance r from the optical axis equal to

$$r = f n_m \sin\theta_m$$

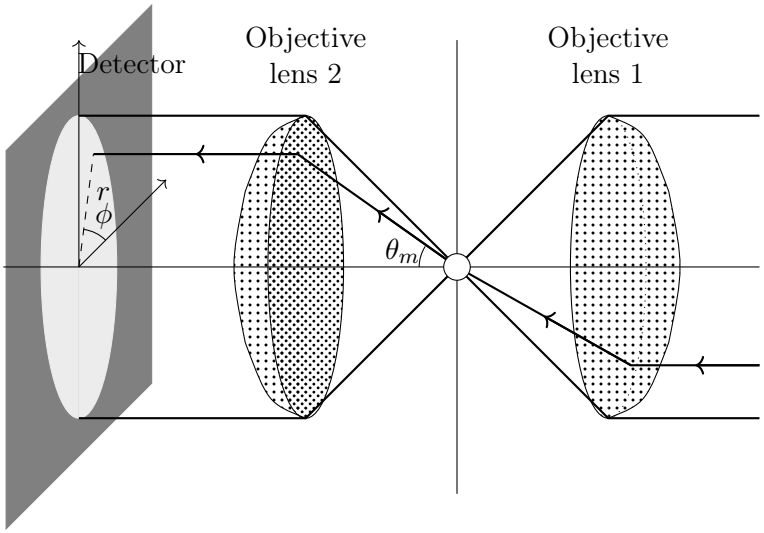

Figure 1.7
Schematic representation of the light signal collected in a detector. The light, after being focused through a first lens, interacts with the sphere and then is collimated again by a second lens. If the ray forms, with respect to focus and the optical axis, an angle θ_m, the Abbe's conditions allow to identify the radius through the angle ϕ and the radius $r = f n_m \sin\theta_m$ with respect to the center of the detector.

where f is the focal length, n_m the refractive index of medium. The Snell's law, $n_m \sin\theta_m = n_{\text{air}} \sin\theta_{\text{air}} = n_{\text{glass}} \sin\theta_{\text{glass}}$, ensures the validity of the formula even when the light beam passes trough different media (as in the experimental case where the light passes through the glass of the coverslip, the water and the lens). If the rays, coming out of the trap in a small element of solid angle $\mathrm{d}\Omega$, are projected without any loss into an area element $\mathrm{d}\Sigma = r\ \mathrm{d}r\,\mathrm{d}\phi$ of the lens principal plane, then from the energy conservation it could be introduced the irradiance, or light intensity, $\mathscr{E}(r,\phi)$ $(\frac{\mathrm{W}}{\mathrm{m}^2})$ given by:

$$\mathscr{E}(r,\phi)\ \mathrm{d}\Sigma = \mathscr{I}(\theta,\phi)\ \mathrm{d}\Omega$$

These terms in the equation (1.18) gives:

$$\mathbf{F}_p = \frac{1}{c}\int_S \mathscr{E}(r,\phi)\left(\hat{\mathbf{x}}\frac{r}{f}\cos\phi + \hat{\mathbf{y}}\frac{r}{f}\sin\phi + \hat{\mathbf{z}}\,n_m\sqrt{1-\left(\frac{r}{f n_m}\right)^2}\right) r\ \mathrm{d}r\,\mathrm{d}\phi \qquad (1.19)$$

The transverse components of the force, that are F_x and F_y, can be inferred based on the relative position of the image generated on a PSD detector (positional sensitive detector). As a matter of fact, the output signals of a PSD detector, D_x and D_y, are proportional to the amount of sum of irradiance, weighed by the relative distance, x/R_D and y/R_D, (where R_D is the half of the detector dimension) from the center of the

detector, and the responsivity Ψ of the device as reported below:

$$D_x = \Psi \int_D \mathscr{E}(x,y)\frac{x}{R_D}\,\mathrm{d}D = \Psi \int_D \mathscr{E}(r,\phi)\frac{r\cos\phi}{R_D}\,\mathrm{d}D \tag{1.20}$$

$$D_y = \Psi \int_D \mathscr{E}(x,y)\frac{y}{R_D}\,\mathrm{d}D = \Psi \int_D \mathscr{E}(r,\phi)\frac{r\sin\phi}{R_D}\,\mathrm{d}D \tag{1.21}$$

Therefore, the values of the force could be obtain from:

$$F_x = \frac{R_D}{c\Psi f}D_x \tag{1.22}$$

$$F_y = \frac{R_D}{c\Psi f}D_y \tag{1.23}$$

Concerning the component of the force along the $\hat{\mathbf{z}}$ axis (that is the propagation direction of the beam), it can be measured by combining the detector with a variable attenuator, with a radial transmission device equals to $\sqrt{1-[r/(fn_m)^2]}$ so that the response of the device is given by:

$$D_z = \Psi \int_D \mathscr{E}(r,\phi)\sqrt{1-\left(\frac{r}{fn_m}\right)^2}\,\mathrm{d}D \tag{1.24}$$

The force component is:

$$F_z = \frac{n_m}{c\Psi}D_z \tag{1.25}$$

In conclusion, it has been demonstrated that it is possible to overcome the theoretical difficulties in deriving the exact value of the force applied to the trapped object via the Maxwell stress tensor, by deriving the trapping force through a direct measure of the beam emitted by the system. In the estimation of radial components there is no dependence nor on the optical properties of the medium (refractive index), or the particle size, neither on the light power used for the creating the trap, thus making this type of measurement versatile and useful in various experimental contexts. On the other the force dependence on the refraction index of the medium n_m cannot be avoided, so attention has to be paid during the calibration process of the instrument. This method is used in the mini optical tweezer apparatus used in this thesis work, which allows to determine and applied forces in the pico newton range.

Chapter 2

Mini-Optical Tweezers Setup

The measuring apparatus used in this thesis takes the name of mini optical tweezers, whose conception is due to Bustamante, Smith et al.[29, 30]. Early prototypes of optical traps were most often built by modifying an inverted microscope so that a laser beam can be introduced into the optical path before the objective: the microscope then provides the imaging, trapping chamber manipulation, and objective focus functions[31]. Usually this solution suffers from some limitations principally due to the high numerical aperture lenses that strongly focalize the single laser beam to create the optical trap conditions. The project by Burstamante and Smith makes it possible to overcome these difficulties and shortcomings. The main features are here summarized. Two counter-propagating laser beams are used to cancel the scattering force and reinforce the gradient component. This allows to optimize the collection of the scattered light, also when the system is not perfectly aligned. Differently from some setup, that uses a substrate to compensate the scattering force of light and then can only measure forces parallels to this surface, all the three components of the force can be measured with this mini-optical tweezer setup. A custom-made handlers, called wiggler, can move the position of the trap by bending the head of an optical fiber. Finally all the apparatus is enclosed in a compact and light box that can therefore be easily isolated mechanically by means of a spring.

2.1 The mini optical tweezer

The mini optical tweezers uses two counter-propagating beams that produce, into a microfluidic chamber, an optical trap in which the scattering force is canceled out leaving only the gradient force. In this configuration, lower beam focusing is required reducing the dispersion of the marginal ray and allowing to use lenses with lower numerical aperture (NA), compared to the case of the single beam. This reduces the problems due to spherical aberrations otherwise present, allow to have longer focal lengths thus focusing the beam deep into the fluidic chamber and finally reducing the heat, harmful to biological systems, released to the medium in which the experiment takes place. Two propagating beams can be used in a decoupled way in single beam experiments, thus forming two independent traps (dual-trap configuration). The main problem, plaguing the system, is the is the necessary alignment achieved through an electronic feedback system.

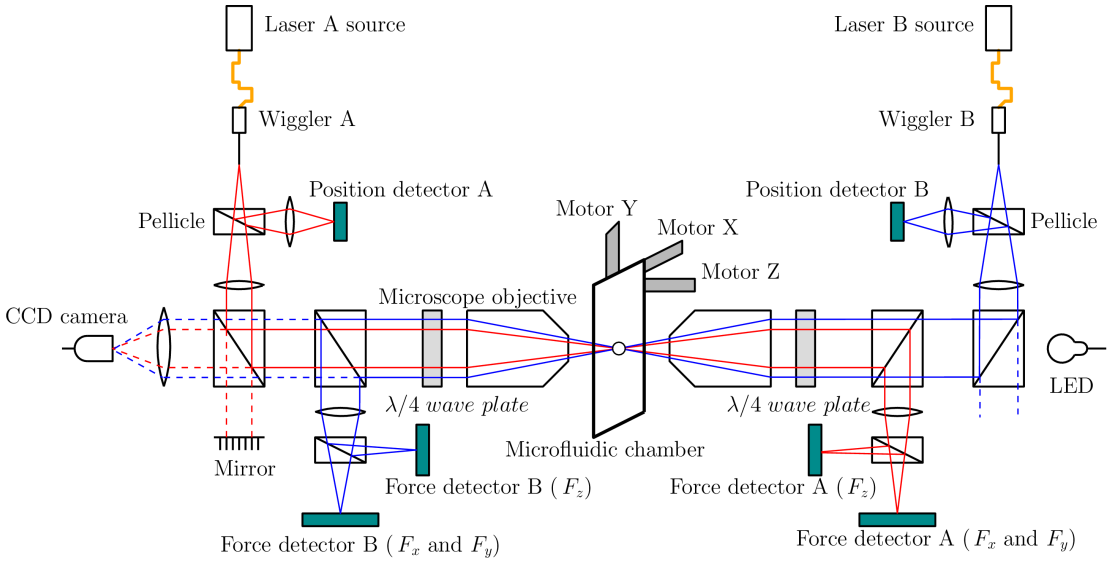

Figure 2.1
Schematic representation of the apparatus with the optical path of the beams and the imaging system.

In the following, for the sake of clarity, it will be analyzed the optical path of one of the two counter-propagating beams, assuming the exact symmetry of the other. The Figure 2.1 illustrates and summarizes che the apparatus and the optical path.

Since most experiments are carried out in water-based solutions which have a minimum of absorption in infrared light, a near infrared light laser was used. The laser diode used (Lumix SN0834770) emits a beam of wavelength $\lambda = 808\,\text{nm}$ up to $200\,\text{mW}$ with TEM_{00} mode with Gaussian linearly polarized intensity profile. The intensity of the beam is measured by a photodiode inside the resonance cavity, while the operative temperature of the laser is controlled by a thermistor and regulated by a thermoelectric cooler using the Peltier effect. The laser diode is coupled with a single-mode optical fiber on which is present a fiber Bragg grating that cleans the signal and transmits a better monochromatic beam. The end part of the fiber is linked to the wiggler, the device used for spatial handling the optical trap. This consists of two coaxial brass tubes: on the inner tube, the optical fiber is fixed in order to keep it straight, while its free terminal part exceeds the length of the outermost tube exposing the fibre head and allowing to bound the fiber to the external tube(see Figure 2.2). The system is fixed to support equipped with two piezoelectric actuators which allow moving the optical fiber head in the plane orthogonal to the propagation direction of the beam with a maximum excursion of $11\,\mu\text{m}$, which results in a numerical aperture of 0,12.

The light exiting from the fiber encounters a beam-splitter pellicle that divides it into two parts: 5% of the beam is directed towards an aspherical lens (which allows to focus divergent beams without introducing aberrations) and then intercepts a positional sensitive detector (PSD) used to determine the position of the trap generating a signal called *light-lever*; the remaining 95% of the light is collimated and directed along the main optical path where the trap will be formed.

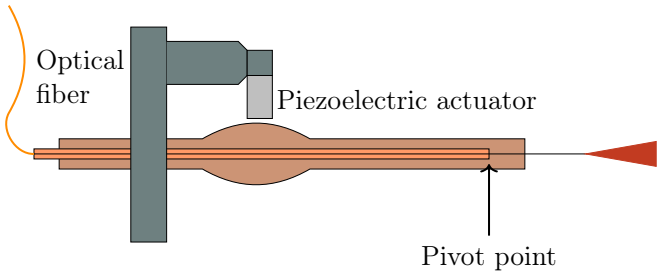

Figure 2.2
Schematic representation of the wiggler, the device used for spatial handling, along two dimension, of the optical trap.

The beam continues towards a first polarizing beam-splitter (PBS) that allows light to be transmitted or reflected depending on polarization. The horizontal component of the polarization is selected and reflected to a quarter-wave plate that produces a circular polarization.

The beam is focused by an immersion lens (Olympus UPLSAPO 60×, with numerical aperture NA= 1,2) to form, inside a microfluidic chamber, the optical trap. The emerging light is collected by a second immersion lens identical to the first one and directed towards a second quarter-wave plate that produces a vertical polarization. The presence of the quarter-wave plates is useful in order to have circular polarization for both beams in the region where the optical trap is formed. In this way the force of the trap is independent of polarization because equally composed by vertical and horizontal polarized light. However, in the optical path external to the hight numerical aperture objectives, the beams presents reciprocal orthogonal polarization that prevent interaction between them.

After the second objective, the collected light is sent to a series of optical components (mirrors and beam splitters) which allow directing it to a PSD and a photodiode(OSI optoelectronics, PIN-10DI) combined with a bullseye filter: these two detectors are used to obtain the transverse components of the force (F_x and F_y) and the axial one (F_z), respectively.

The experiment can be observed through a microscope made from a CCD camera (Watec WAT-902H3 SUPREMA EIA) and a LED light ($\lambda = 470\,\text{nm}$) expanded with a lens in order to produce a Köhler illumination system in the region of the focal plane, so the target is evenly illuminated without making the light source visible.

The CCD camera is monochromatic and sensitive in the visible and near infrared. Both the sample and the optical trap are therefore visible. Because the intensity of the latter saturates the signal making invisible everything around this region, an infrared filter is placed before of the camera with the possibility of be inserted or removed. In this way, the beam does not intercept the CCD and all the elements of the microfluidic chamber and the samples are perfectly visible during the experiments. In laser alignment operations, however, the filter is removed in order to see the two lasers.

The experiment takes place in a microfluidic chamber fixed on a motorized stage moved by triaxial stepper motors that allow the handling of the chamber along the three axes.

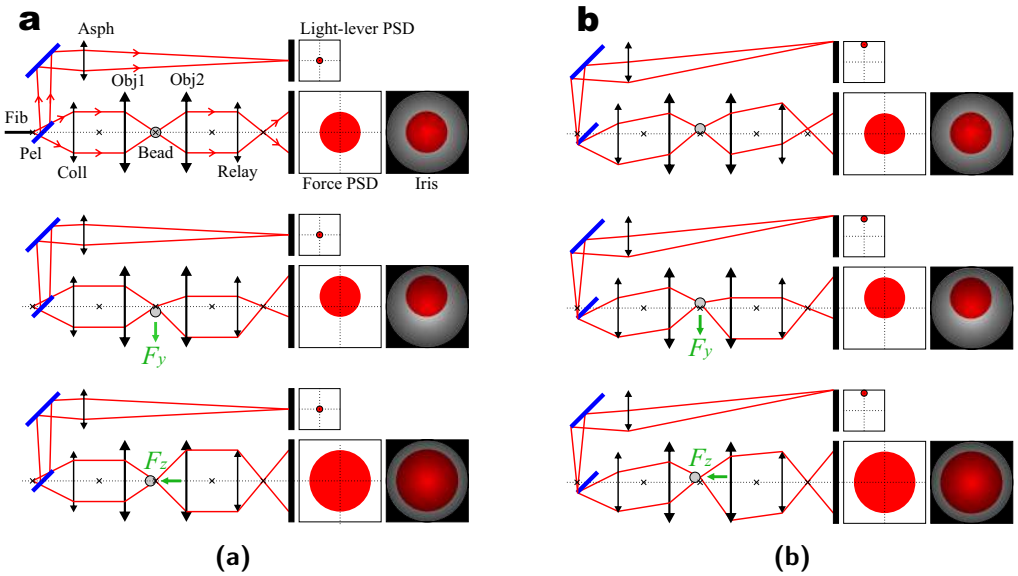

Figure 2.3
Diagram of the working principle of the detection of the signals of position and force of the optical trap. In (a) the position of the centroid coincides with the center of the PSD of the light-lever, therefore the relative position of the trap turns out to be zero, even if a force, along F_y or F_z, are applied. This two component can be reveal by the force PSD and the photodiode through a signal called Iris. When the trap is moved, using the wiggler, it only affect the signal of the light-lever PSD as can be see in (b).

The center of the both position and force detectors are taken as reference, so that any displacement of the beam centroid with respect to it means that the trapped has been moved or/and a force has been applied to the object. In particular, if no forces are applied to the trapped object (see Figure 2.3 first row), any movement of the trap results in a displacement of the beam only in the position detectors, whereas the beam remains at the center of the force detectors. On the contrary, if by moving the optical trap a transverse force is applied to the object (Figure 2.3 second row), a displacement of the beam centroid with respect to the detector center is observed both in the position and in the force detectors. Finally, when a longitudinal force (F_z) is applied (Figure 2.3 third row), the radius of the beam behind the trapped object increase(decrease), so that the beam is more (or less) attenuated by the bullseye filter and the light intensity recorded by the F_z-detector varies.

2.2 The acquisition systems

The electronics of the apparatus allows to acquire the displacement of the position of the light spot on a detector on the focal plane, and this signal will be called *light-lever*. Similarly, from the displacement of the scattered light can be inferred the value of the force that causes the variation of the momentum of the light. The signal will be called *force PSD*, for the transverse forces signals F_x and F_y, and *iris* for the axial component

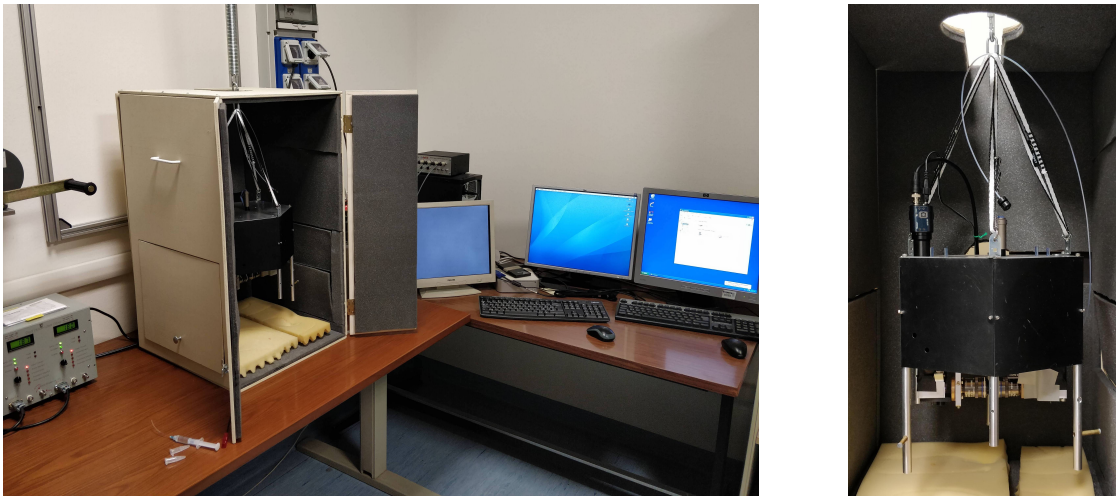

(a) **(b)**

Figure 2.4
The optical tweezer setup (a) and the apparatus (b).

F_z. Below it will be described the working principle of the devices and the main electronic components used to extract the signals.

Positional sensitive detector. The positional sensitive detector (PSD) is a optoelectronics device that produce an electric signal proportional to the displacement of the centroid of the incident beam on the sensible area of the detector. It consists of a diode PiN between two conductive plates each one with two electrodes opposite each other. The diode is fed in reverse polarization mode: the layer P is held at negative voltage, while the layer N in positive. When the stream of photons interact with the intrinsic zone of the diode it produces pairs of electron-hole traveling in opposite directions through the conductive layer. This induces a current in the diode proportional to the distance between the spot, point of origin of the pairs, and the electrode; from the current intensity the distance from the centre of the detector can be inferred. Starting from the signal D_x that is the difference of the upper plate currents (I_l and I_e) it is possible to get the position along the direction $\hat{\mathbf{x}}$, while the component $\hat{\mathbf{y}}$ is given by the signal D_y obtain as difference of the currents of the lower plate I_t and I_b, by the following equations:

$$D_x = I_l - I_r = \Psi \int_D \mathscr{E}(x,y)\frac{x}{R_D}\,\mathrm{d}D \tag{2.1}$$

$$D_y = I_t - I_b = \Psi \int_D \mathscr{E}(x,y)\frac{y}{R_D}\,\mathrm{d}D = \tag{2.2}$$

where $\mathscr{E}(x,y)$ is the irradiance on the surface D of the detector of dimension $2R_D$. The sum of the currents, on the other hand, provides the information on the total intensity reaching the sensors.

Since the apparatus uses two lasers the total force could be calculated using the equations (1.22) and (1.23) where the position is the sum of the displacement of the spot of the laser:

$$F_x = \frac{R_D}{c\Psi f}(\Delta D_{x_1} + \Delta D_{x_2}) \tag{2.3}$$

$$F_y = \frac{R_D}{c\Psi f}(\Delta D_{y_1} + \Delta D_{y_2}) \tag{2.4}$$

where R_D is the half of the dimension of the detector, Ψ is the efficiency of the detector, f is the focal length and ΔD is the variation of the signal with respect to the starting value taken as reference, which usually correspond to.

Photodiode To obtain the longitudinal force, along the optic axis, F_z a photodiode is used for monitoring the light of incident beam. As shown earlier, to obtain the value of the force, is necessary match the scattered light intensity with an attenuator with a circular transmission profile (the bullseye filter) described by the transmission coefficient T:

$$T(r) = \sqrt{1 - \left(\frac{r}{nf}\right)^2}$$

where r is the distance form the center of the detector. The response of the detector for a ray with irradiance $\mathscr{E}(z)$ will be

$$D_z = \Psi' \int_D \mathscr{E}(r,\phi)\sqrt{1 - \left(\frac{r}{fn_m}\right)^2}\,\mathrm{d}D$$

where Ψ' is the responsivity of the photodiode. The measure of the force will be:

$$F_z = \frac{n_m}{c\Psi'}(\Delta D_{z_1} - \Delta D_{z_2})$$

In order to compensate the differences in laser powers and sensitivities, the difference signal $(\Delta D_{z_1} - \Delta D_{z_2})$ is nulled by an offset, before any particle enters the trap.

Foci position feedback. Room temperature and humidity can compromise the alignment of all optical parts, while the dual counter-propagating beams requires constant alignment in order to keep the foci coincident. The misalignment compromise the stiffness of the trap, but also produces artifacts in the force signal. Any misalignment in the focal plane can be correction can be performed using an *auto-align* command performed by the wiggler, while the axial correction is obtain manually moving the focal length of one of the two focalizing objective lens.

While an external transverse force on the trapped particle deflects both exiting beams in the same direction, a transverse misalignment of the foci cause the exit beams to be deflected in opposite direction. Because the transverse alignment is proportional to the difference of the position signal:

$$x - \text{error} = \Delta D_{x_1} - \Delta D_{x_2}$$
$$y - \text{error} = \Delta D_{y_1} - \Delta D_{y_2}$$

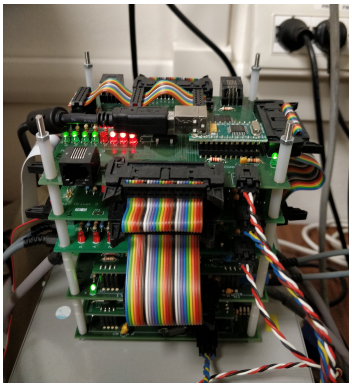

(a)

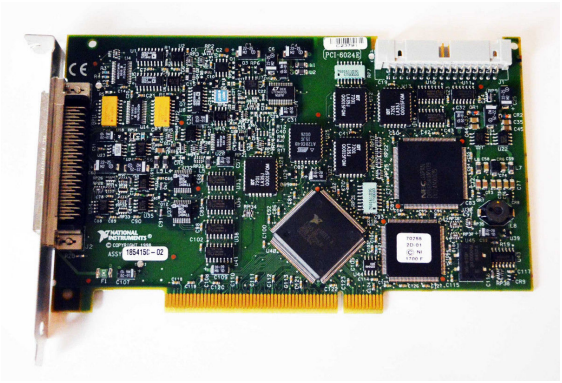

(b)

Figure 2.5
The optical tweezers are controlled by an electronic board (a) that interface the apparatus with an host computer and allows to control the motion of the chamber and extracts the signals related to the position of the trap ($\hat{\mathbf{x}}$,$\hat{\mathbf{y}}$) and the force components (F_x, F_y and F_z). For high frequency acquisition a second board (b) was used, which derives from the first the transverse positions and forces ($\hat{\mathbf{x}}$, $\hat{\mathbf{y}}$, F_x, F_y).

the information useful to correct the alignment error may be derived form this formula. This signal is processed by a proportional-integrative-differential (PID) feedback algorithm that moves the piezo electric actuators of the wiggler in order to vanish the displacement.

The axial misalignment, namely the non null distance between the foci along the optical axis, can be reveal by an increasing or decreasing of the signal through the photodiode. The error, in this case, can be derived from the comparison of the sensor outputs with a particle in the trap, $(D_{z_1} + D_{z_2})_{\text{full}}$ and the same measure while the trap is empty, $(D_{z_1} + D_{z_2})_{\text{empty}}$. However the "empty" measurement would need to change if the laser power changes with time. Therefore it is necessary to normalize the ΔD_z signals by their respective laser powers (Sum):

$$z - \text{error} = \left(\frac{D_{z_1}}{\text{Sum}_1} + \frac{D_{z_2}}{\text{Sum}_2}\right)_{\text{full}} - \left(\frac{D_{z_1}}{\text{Sum}_1} + \frac{D_{z_2}}{\text{Sum}_2}\right)_{\text{empty}}$$

Electronic control and acquisition. The electronic control manages the communication and acquisition of the different signals sent and received by the apparatus of mini optical tweezers. In particular it deals with the photodetectors and the management of the piezoelectric actuators and the motors of the chamber and it sends and receives data from an host computer. It is composed by an ADC card (analog to digital converter) that digitizes the current signals of the PSD (position and force) obtained from a pre-amplifier stage that deals with the readings of the current I_r, I_l, I_t and I_b from which it then derives the position, $\hat{\mathbf{x}}$ and $\hat{\mathbf{y}}$, and the total intensity (in the software this magnitude is indicated as "PSD sum"). A digital to analog converter (DAC) card converts the digital trap displacement signal into a voltage applied to the piezoelectric crystals that move the wiggler. Finally, a last card controls the movement of the step-by-step motors of the

Parametri	Valori	
Analog data bandwidth	1	MHz
PIC internal clock	10	MHz
Sampling rate	4	kHz
Feedback running frequency	4	kHz
Digital data bandwidth	1	kHz
ADC force resolution	0.01	pN
Maximum detectable force	400	pN
ADC distance resolution	0.1	nm
Maximum detectable distance	12	µm
Piezo update frequency	4	kHz
Wiggler relaxation time	< 1	ms

(a)

Gain	Input range	Precision
0,5	−10 to 10 V	4,88 mV
1,0	−5 to 5 V	2,44 mV
10,0	−500 to 500 mV	244,14 µV
100,0	−50 to 50 mV	24,31 µV

(b)

Table 2.1
Specifications of the electronic controller of the mini optical tweezers (a) and the gain and precision of the high frequency board (b).

chamber as well as it records the actual displacement allowing to determine the position of the motors. In this way it is possible to save and recall prefixed positions using the optical tweezer software. In Table 2.1a the main technical features of this first control board are collected. As it can be observed, the sampling rate of this card is 4 kHz, but in force spectroscopy measurements, such as the one presented in this work, an higher sampling rate is necessary.

High frequency data acquisition board. In order to be able to perform high frequency measurements (for example 50 kHz) it was necessary to implement a second electronic board into the optical tweezers setup. A data acquisition board is directly connected to the optical tweezers board, thus allowing to record with an higher frequency the signals relative to both the position and the force detectors. In particular, only the transverse components of the forces can be recorded (i.e F_x, and F_y) and by means of a custom made program it is possible to control the gain of the data acquisition (see Table 2.1b). The sampling rate is variable and its maximum value is 200 kHz, the data used for this thesis were acquired with a sampling rate of 50 kHz.

2.3 Microfluidic chamber

All of the biological experiments have to take place into liquid medium, called buffer. This makes it necessary to use a microfluidic chamber (see Figure 2.6a). It is build from two coverslips (whose dimensions are: 24 mm × 60 mm × 150 µm) separated by two identical parafilm masks (see Figure 2.6f)

On one of the coverslips three pair of holes are drilled, using a sandblasting machine (Dentalfarm, dry oxide WAFIS, alluminiabis) that blasts aluminum oxide (Al_2O_2) with

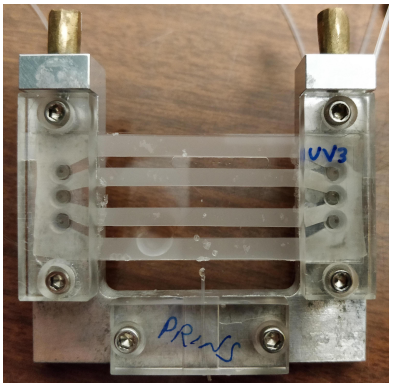

(a)

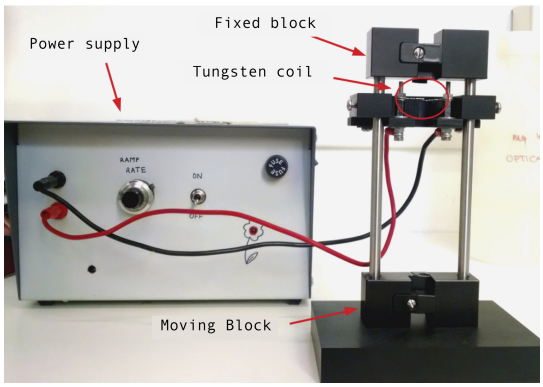

(b)

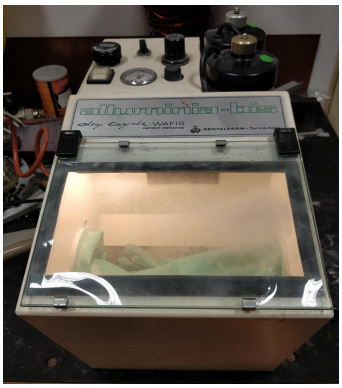

(c)

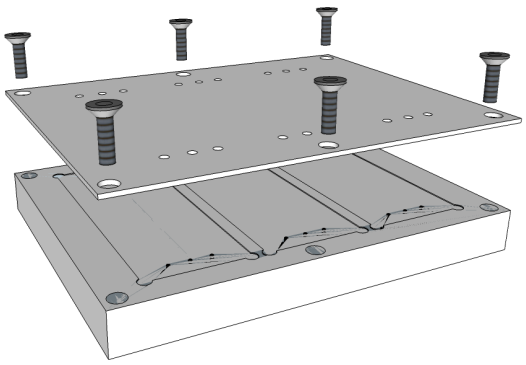

(d)

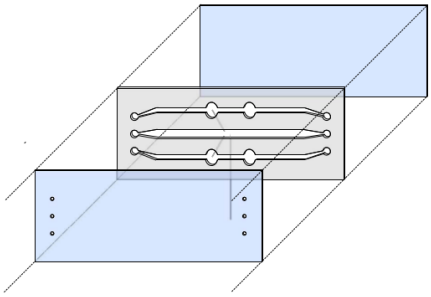

(e)

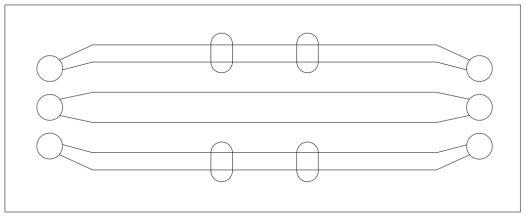

(f)

Figure 2.6
The microfluidic chamber (a). The sandblasting (c) and the mask used to drill che coverslips (d). The microfluidic chamber is composed by two coverslips and two Parafilm strips with glass capillary used to connect che channel on the mask (e). The profile of the Parafilm mask (f). The pipette puller used to forge the micro pipette (b).

a pressure of 4 bar on an home-made aluminum mask where the coverglasses are inserted. The diameter of the holes are approximately of 1 mm (see Figure 2.6c).

Two Parafilm strips are designed to create three channels that connect the entering holes with the exit ones fluidic channel were the experiments are carried out. They are realized with a cutter that reproduce the mask showed in Figure 2.6f. The upper and the lower channels are connected to the central one by two dispenser tube, a capillary (King precision glass Inc.) positioned transversally between the external channels and the one in the middle. Their smaller dimension (the external diameter is $\phi_e = (0{,}100 \pm 0{,}010)$ mm and the internal one is $\phi_i = (0{,}0400 \pm 0{,}0064)$ mm) compared with the wide of the channel (some millimeter) allow to introduce in the central channel a small amount of buffer and beads injected in the lateral channel. At the center of the chamber is placed a micro pipette created starting from a capillary (King precision glass Inc., $\phi_e = (0{,}080 \pm 0{,}010)$ mm and $\phi_i = (0{,}0400 \pm 0{,}0064)$ mm) which is melted and extruded through the use of a pipette puller (see Figure 2.6b). The pipet puller is a custom made instrument made up of two blocks the lowest of which can move along vertical guides while the other is fixed and resents a tungsten coil in the middle. The capillary is fixed on that blocks passing through the center of the coil which is heated by the Joule effect produced by electric current provided by a 1,5 V power supply. While the power supply is switched off the weight of the moving block is mechanical compensate thanks to the tensile strength of the capillary, but when the coil become incandescent the glass melts and the lower block fall down extruding the micro-pipette. Some empirical aspects affect the profile and the dimension of the pipette, as the diameter and the distance of the windings of the coil and the alignment of the axis of the capillary with the center of the system. Another degree of freedom is the possibility to modify the rampe rate of the voltage, provided by the power supply using a potentiometer; the result is a changing in time of how fast the tungsten, an so the glass, is warm up. It turns out that the higher the ramp value, the smaller the diameter of the pipette. Moreover, the ideal diameter of the tip of the pipette is around 2 µm in order to avoid its obstruction due to undesired substances present in the chamber.

Once the chamber has been assembled, the main problem is the adhesion of the parafilm with the glass of the coverslip, which often causes buffer leakages. In order to avoid this, various strategies had been considered. First of all was changed the temperature of sealing, form 90 °C to $110 - 120$°C but the parafilm melted too fast closing the hole and the channel. An UVO cleaner (Jelight Company, Inc.) was used to activate the surface of the glass, but nor this was sufficient. Finally the coverglasses was coated with a thin film of NOA (Norland Products, Norland Optical Adhesive N. 68) following the shape of the parafilm. After the cure with UV treatment, the chamber was usually composed and sealed at 90 °C. This particular method seems to produce durable supports.

The chamber is anchored between the objectives of the optical tweezers using a "U" shaped aluminum frame (see Figure 2.7) that can be moved along the three dimensions. Three syringe are connected to the chamber while the exit holes collect all the material in a waste reservoir. The upper and the lower channels are exploited to introduce the two beads that are used to manipulate the DNA, whereas the central one is used to clean the experimental area and for this reason the syringe that flux the cleaner buffer presents

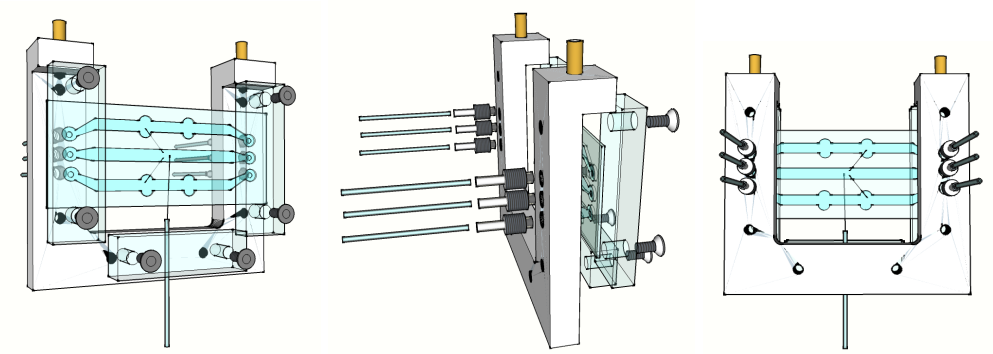

Figure 2.7
A "U" shaped frame used to anchor the microfluidic chamber between the objectives of the optical tweezers.

a 0,2 µm filter to avoid contamination. The micro pipette is connected with an empty syringe in order to realize the suction thus holding the bead in place.

2.4 Buffer

Biological experiments have to take place in salted aqueous solutions, called buffer, in order to prevent the degradation of the polymeric chain. For the experiment with DNA the buffer is composed by: 1 M of sodium chloride (NaCl), 10 mM Trizma® base ($C_4H_{11}NO_3$), 1 mM of Ethylenediaminetetraacetic acid (EDTA) and 0,01% Sodium azied (NaNa). The pH of the solution must be kept around 7,5. The role[32] of the EDTA is to inhibit nuclease, an enzyme capable of cleaving the bonds between nucleotides of the nucleic acids. The Sodium azide prevents the microbial growth in the buffer.

2.5 Beads and incubation

The mechanical manipulation of the DNA requires some preliminary steps in order to link the molecule to mesoscopic particles that will be trapped by the laser or the micropipette.

Each end of the DNA presents at one end the Biotine and on the other side the Digoxigenin. This have the property of instaurate strong and selective bonds with specific molecules: the Digoxigenin[33] is a hapten, a small molecule with high antigenicity, that is used in many molecular biology applications and creates strong bonds with its antigene, the Antidigoxigenin. Biotin[34] is a water-soluble enzyme co-factor presents in minute amounts in every living cell, that strictly bonds to Streptavidin.

Polystyrene particles (Kisker Biotech GmbH & Co., PC-PG-3.0) with a diameter of 3,1 µm are centrifugated and suspended in DMP cosslinker, a chemical compound that promotes the bond between polymeric chains. The protein G coating on the surface of the bead reacts when Antidigoxigenin is introduced in the system. After an hour of incubation, the compound is centrifuged and suspended on phosphate-buffered saline (PBS), a buffer solution used for dilutions. The surface of the particle, now, is functionalized

Length of DNA	DNA	AD	Buffer
24 kbp	2,5 µL	4,5 µL	13 µL
9 kbp	2,5 µL	4,5 µL	13 µL
3,6 kbp	2,5 µL	4,5 µL	13 µL

Table 2.2
The table report the concentration of the DNA molecules (already diluted with ratio 1:10), the AD and the buffer.

with the Antidigoxigenin, an in the following those beads will be called with the acronym "AD".

The other type of beads are streptavidin-coated polystyrene particles (Kisker Biotech GmbH & Co., PC-S-2.0) with a diameter of 2,0 µm. Hereafter those particle are mentioned with the acronym of "SA".

The DNA enters in the system carried by the AD particle. In the preparatory part of the experiment, a dilution of DNA molecules (ratio 1:10), the AD particles and buffer are mixed and left to react during an incubation period of 15 minutes. The Digoxigenin, present at the end part of the DNA, reacts with its antibody, and the concentration ratio of the reagents is tuned in order to bound only some molecules to the surface, to be able to catch only few molecule during the experiment. The dilution ratio used in this work are reported in Table 2.2. After this incubation time, 1 mL of buffer is added to the solution in order to avoid further reactions between the molecules and the beads.

2.6 Calibration of apparatus

The electric signals of the detector have to be converted into physical value, using parameter obtain by the calibration process so called *Stokes calibration*. A subsequent calibration was performed in order to convert the digital signal of forces acquired from the hight frequency board, with the real value of force (in pN), read from the optical tweezer. Finally a third method was use to independently derive the previous calibration factors and also the stiffness of the optical trap, by studying the Brownian motion of a bead inside the optical trap.

Stokes calibration It is well known from the fluid mechanics, that a homogenous and smooth sphere with radius a moving with a velocity v a fluid of density ρ and dynamic viscosity η, is subjected to a drag force F. If the fluid is in a creeping flow regime, so it's characterized by low Reynolds' number $\mathscr{R}$

$$\mathscr{R} = \frac{\rho d v}{\eta} \ll 1$$

the force can be calculated as

$$\mathbf{F} = -6\pi\eta a\mathbf{v} \tag{2.5}$$

known as Stoke's law, which correlates the velocity with the drag force. Therefore, by knowing the viscosity of the fluid and the size of the bead and by moving this latter at a

well defined velocity inside the chamber, it is possible to calculate the Stokes force acting on the bead (in pN) and use this value to calibrate the electronic signal measured by the optical tweezers. To this aim, a calibration bead, a sample sphere whose diameter is well known, $2a = (3{,}00 \pm 0{,}02)\,\mu m$, is trapped into the well potential of the optical trap and the chamber is moved along the $\hat{\mathbf{x}}$ or $\hat{\mathbf{y}}$ direction, back and forward, changing average speed.

The signal of the PSDs of the force, the relative position of the chamber and the time are recorded. Using a MATLAB script, the whole signal of Figure 2.8a can be subdivided into sigle displacements characterized by a velocity v, whose exact value can be determined by fitting the corresponding position of the chamber as a function of time. In this way for each investigated velocity it is possible to obtain a mean value of the voltage values recorded by the optical tweezers software, as reported in Figure 2.8. With reference to the equations (2.3) and (2.4) the link between the force and the PDSs signal, $[\mathrm{PSD}]_F$ (the subscript "F" remind that the PSDs are the one used to read the force), is linear and can be described by:

$$F = A \cdot [PSD]_F + B$$

Substituting the Stokes' force (2.5) into the previous equation, it could be obtained:

$$v = \frac{A}{6\pi\eta a}[PSD]_F + \frac{B}{6\pi\eta a}$$
$$v = M[PSD]_F + Q$$

By fitting the data as shown in Figure 2.8, the value of A and B can be obtained:

$$A = 6\pi\eta a M \qquad \sigma_A = A\sqrt{\left(\frac{\sigma_a}{a}\right)^2 + \left(\frac{\sigma_M}{M}\right)^2} \tag{2.6}$$

$$B = 6\pi\eta a Q \qquad \sigma_B = B\sqrt{\left(\frac{\sigma_a}{a}\right)^2 + \left(\frac{\sigma_Q}{Q}\right)^2} \tag{2.7}$$

where $\sigma_a = 0{,}02\,\mu m$ is the statistical deviation the the calibration beads[1], σ_M and σ_Q are the statistical errors of the slope and the intercept, derived from the fitting algorithm. Repeating the same procedure for other beads, it is possible to collect various value of A_i and B_i with the respective errors, and the final value is obtain through weighted averages.

	A $[\frac{\mathrm{pN}}{\mathrm{V}}]$	B [pN]
x-direction	$0{,}0423 \pm 0{,}0004$	$5{,}0391 \pm 0{,}0008$
y-direction	$0{,}0417 \pm 0{,}0002$	$0{,}600 \pm 0{,}004$

Force calibration of high frequency board As already said, the high frequency board extracts, from the main board, the transversal raw signal of position and force for

[1] Factory information

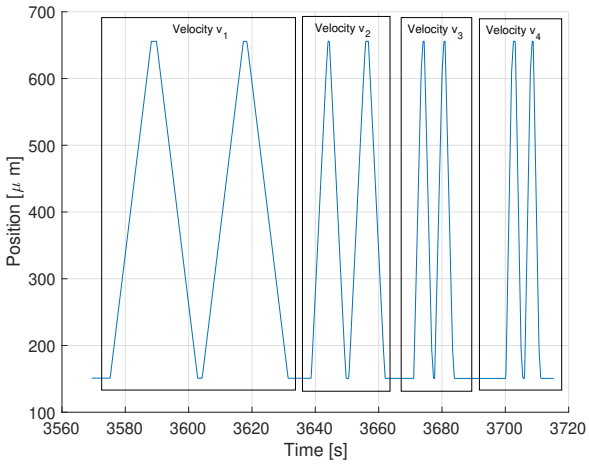

(a)

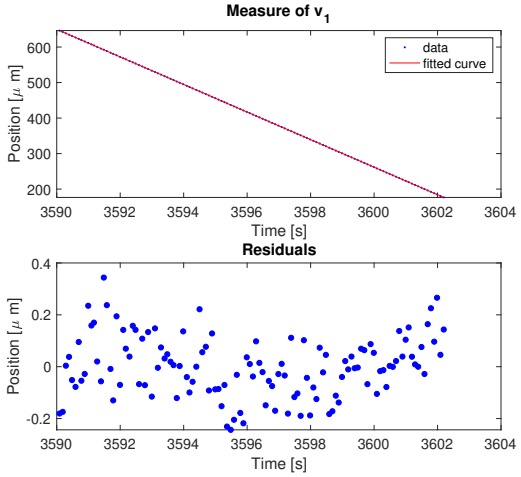

(b)

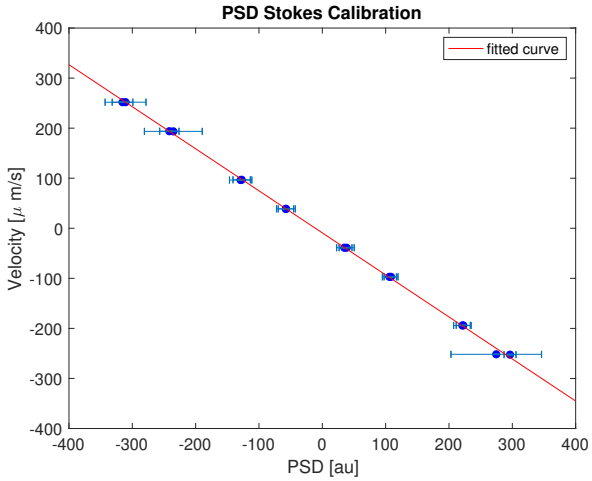

(c)

Figure 2.8
Stokes calibration procedure.

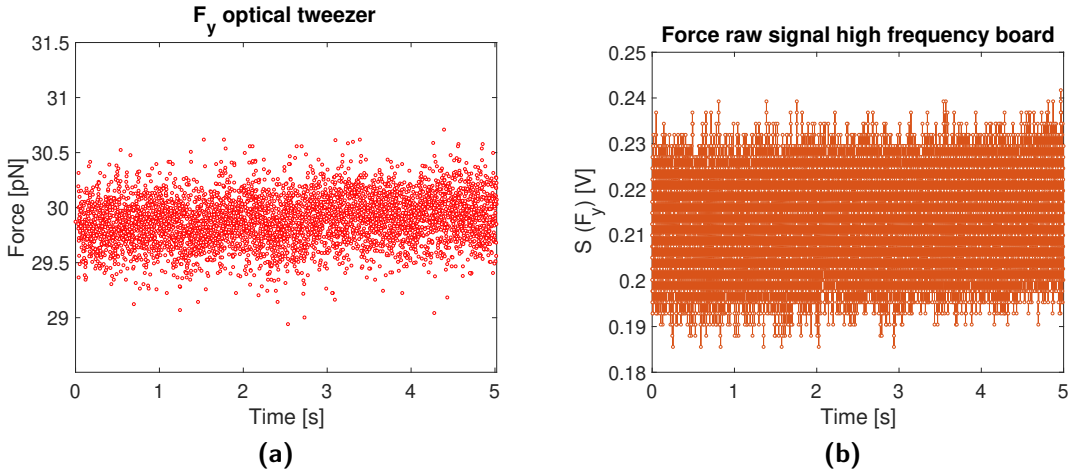

Figure 2.9
The signal of a constant force applied to a single DNA molecule along the $\hat{\mathbf{y}}$ direction, recorded by (a) the optical tweezers board and (b) the high frequency board.

both PSDs, named as $\mathbb{S}_f(\hat{\mathbf{x}}_i)$, $\mathbb{S}_f(\hat{\mathbf{y}}_i)$, $\mathbb{S}_f(F_{x,i})$ and $\mathbb{S}_f(F_{y,i})$, for both the lasers $i = 1, 2$. The data conversion, from the raw signal to the physical force, is necessary and can be performed even with the absence of the axial force component. For sake of clarity, in the following only the calibration of the $\hat{\mathbf{y}}$-component of the force will be presented in details.

The experimental protocol, indeed, required the acquisition of only one of the two component of the force; in particular, when a DNA molecule is linked between the two beads, it was subject to a force along only the $\hat{\mathbf{y}}$ direction, achievable by moving the trap, or the micro-pipette (i.e. the chamber), and removing the other force component by controlling the value on the optical tweezer software. In this way the system could be considered as unidimensional, along the $\hat{\mathbf{y}}$ direction, and only one calibration is necessary.

The calibration was performed by applying a constant force to a DNA molecule tethered between two beads and by simultaneously recording the force values on both the optical tweezers board and the high-frequency one (see Figure 2.9). Their mean values were reported into a graph and interpolated with a linear fit estimating the slope M and the intercept R. In this way the calibration could be performed using the formula:

$$F_y = M_y \langle \mathbb{S}_f(F_{y,1}) + \mathbb{S}_f(F_{y,2}) \rangle + R = M_y \langle \mathbb{S}_f(F_y) \rangle + R$$

where $\langle\,\rangle$ is the time averaging. The high frequency board allows to record signals with different gain, so the data acquisition was performed with a gain value ranging from 1 to 10. The results are reported in Figure 2.10 where it is possible to observe as a deviation from the linearity appears at high force when a low gain is used, due to the signal saturation (Figure 2.10b). The conversion parameters are reported in the following table.

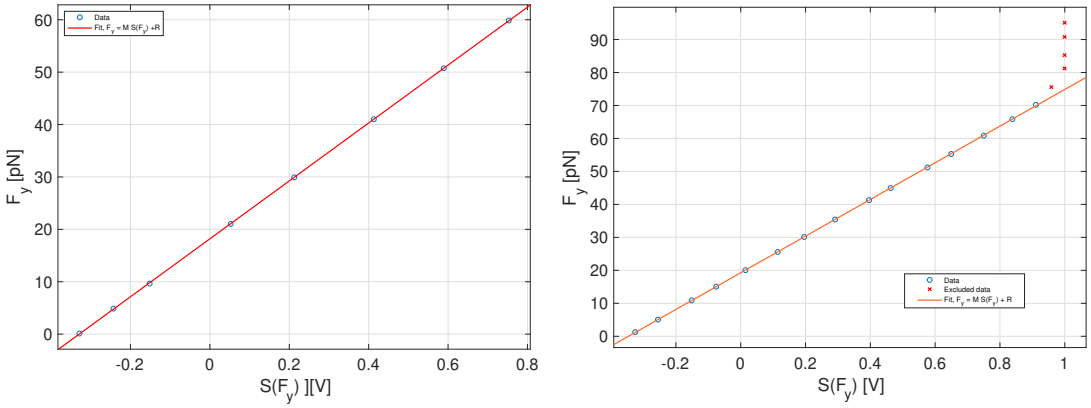

Figure 2.10
The graphs report the linear correlation between the signal recorded via the high frequency board, $\mathbb{S}_f\, F_y$ and the force measured by the tweezer software, F_y, with different gain: 10,0 for (a) and 1,0 for (b). For the latter is possibile to see the saturation of signal express as deviation form linearity near 1 along the abscissa.

	Gain=1	Gain=10
M_y $[\frac{\text{pN}}{\text{V}}]$	$55{,}2 \pm 0{,}2$	$55{,}6 \pm 0{,}2$
R [pN]	$18{,}19 \pm 0{,}09$	$19{,}26 \pm 0{,}07$

In the following, in order to avoid systematic error in the calibration and knowing that the power spectrum, as show later, will not depend on R, except for the continuous component (i.e. frequency $f = 0$), it is useful performing a differential measure recording the zero force signal at the beginning of each measure without any molecule attached between the two beads. With this method the conversion could be performed in this way:

$$F_y = M_y \langle \mathbb{S}_f(F_y) - \mathbb{S}_f(0) \rangle \tag{2.8}$$

Calibration via power spectrum Another way to get the conversion parameter M_y is by means of the power spectrum analysis of the force signal recorded by the high frequency board. As a matter of fact, the motion of a sphere (of radius a) trapped in a optical tweezer of stiffness k and immersed in a fluid of viscosity η, with a drag coefficient $\gamma = 6\pi\eta a$, at temperature T, is described by the Langevin's equation in overdamped regime ($\gamma \gg 0$):

$$kx(t) + \gamma\dot{x}(t) + \sqrt{2\gamma k_B T}\xi(t) = 0$$

where $\xi(t)$ describe a gaussian process that represent the brownian forces acting on the sphere. Through the Fourier's transformation, the differential equation can be rewritten in the following way:

$$k\widetilde{x}(\nu) - i2\pi\nu\gamma\widetilde{x}(\nu) + \sqrt{2\gamma k_B T}\widetilde{\xi}(\nu) = 0$$

The position, in the frequency domain, is:

$$\widetilde{x}(\nu) = \frac{\sqrt{2\gamma k_B T}}{k - i2\pi\gamma\nu} \tag{2.9}$$

The force acting on the sphere, an so indirectly on the DNA molecule, could be obtained multiplying the displacement by the stiffness:

$$\widetilde{F_y}(\nu) = k\widetilde{x}(\nu) \tag{2.10}$$

The power spectrum of the time average of the force is defined by:

$$\mathbb{P}_{F_y}(\nu) = \langle \widetilde{F_y}^*(\nu)\widetilde{F_y}(\nu)\rangle$$

where $\widetilde{F_y}^*$ is the complex conjugate of the Fourier's transformation of the force. By replacing the definition of the force (2.10) and the position (2.9) it can be found:

$$\mathbb{P}_{F_y} = \frac{2\nu_c\gamma k_B T}{\nu_c^2 + \nu^2} \tag{2.11}$$

where the corner frequency ν_c is define as:

$$\nu_c = \frac{k}{2\pi\gamma}$$

The signal acquired, $\mathbb{S}_f(F_y)$, will follow the same lorentian shape given by (2.11) and the conversion, as already said, is given by[2]:

$$F_y = M_y\,\mathbb{S}_f(F_y)$$

so the power spectrum of the raw signal can be describe by:

$$\mathbb{P}_{\mathbb{S}_f(F_y)}(\nu) = \frac{A}{B^2 + \nu} \tag{2.12}$$

The calibration formula allow to combine the two power spectra:

$$\mathbb{P}_{F_y}(\nu) = M_y^2\,\mathbb{P}_{\mathbb{S}_f(F_y)}(\nu)$$

and from that it's possible to obtain M_y and the stiffness of the trap k:

$$M_y = \sqrt{\frac{B^2}{A}12\pi\eta a k_B T} \tag{2.13}$$

$$k = 12\pi^2\eta a B \tag{2.14}$$

[2]In this discussion the null force term, namely $\mathbb{S}_f(0)$, and the time average will be neglected in order to maintain a clear formalism. The final result would be the same even if one uses the conversion formula: $F = M_y\,\mathbb{S}_f(F_y) + R$ since the constant R is absorbed in the DC component ($f = 0$) of the spectrum, due the Fourier's transformation: $\widetilde{F} = M_y\widetilde{\mathbb{S}_f(F_y)} + R\delta(\omega)$

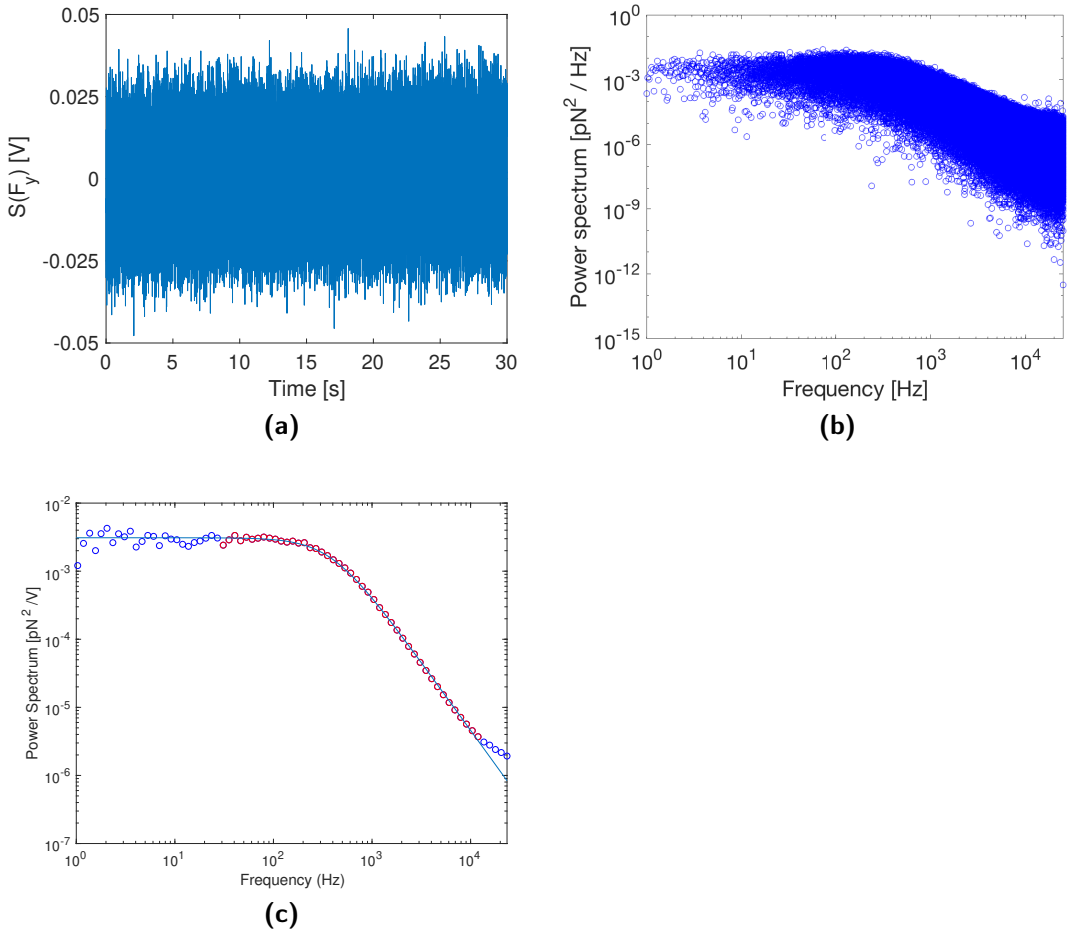

Figure 2.11
In order to extract the stiffness of the trap and the conversion parameter to calculate the force, a well-known radius bead was trapped in the optical tweezer and recorded its brownian motion. The raw signal ((a)) was plot in a log-log graph ((b)) and mean inside frequency windows. The data was fit with a lorentan curve ((c)).

The calibration was performed using a calibration bead, with radius $a = (3{,}00 \pm 0{,}02)$ µm, trapped in the optical tweezer. Without applying any force, a 30 s recording using the high frequency board was performed (see Figure 2.11a) and the data collected were plotted in a log-log graph (see Figure 2.11b) in order to window the signal and take the mean value inside each subset of data; then the lorentzian fit was performed with the formula (2.12). From the parameters A and B of the fit, the conversion term M_y and the stiffness of the trap k were obtained. The results are shown in the following table:

M_y	pN/V	51,2	$\pm$ 0,1
k	pN/nm	0,060	$\pm$ 0,001

The last characterization of the apparatus was the measure M_y and k as a function of the the power of the two lasers. The signal were recorded for different values of the lasers powe, and the data collected were analyzed in the same way as presented before. The results are summarized in following table and the conversion factor M_y remains constant within 6%, expect for the value relative to the lower laser power, where the light intensity of the laser is so low that its voltage value is significantly affected by the electronic noise of the instrument. Finally, it is possible to observe as the stiffness of the trap decreases.

Laser A [mA]	Laser B [mA]	$M_y[\frac{\text{pN}}{\text{µm}}]$	$k[\frac{\text{pN}}{\text{nm}}]$
187	180	$52{,}2 \pm 0{,}2$	$0{,}060 \pm 0{,}001$
100	103	$55{,}4 \pm 0{,}6$	$0{,}018 \pm 0{,}001$
187	0	$55{,}1 \pm 0{,}3$	$0{,}030 \pm 0{,}002$
140	0	$55{,}5 \pm 0{,}6$	$0{,}018 \pm 0{,}002$
100	0	$62{,}1 \pm 0{,}5$	$0{,}0085 \pm 0{,}0009$

Chapter 3

The biological system

Nearly all living cells store their genetic information in the DeoxyriboNucleic Acid (DNA). Although each organism's DNA is unique, all DNA is composed of the same nitrogen-based molecules. What makes individuals different is how these smaller molecules are arranged. Nucleotides are the basic elements of the DNA and they are composed of three primary components: a phosphate group, a carbon-base pentose sugar, called deoxyribose, and nitrogenous base. There are four different DNA nucleotides, each defined by a specific nitrogenous base: adenine (often abbreviated "A"), thymine ("T"), guanine ("G"), and cytosine ("C"). Although nucleotides derive their names from their nitrogenous bases, deoxyribose molecule is the one defining their structure and bonding capabilities. The central portion of this molecule contains five carbon atoms arranged in a ring shape and each carbon is referred by a number followed by the prime symbol (’). On the 5’ carbon atom is attached the phosphate group and the 3’ joins to the phosphate group of another nucleotide through a phosphodiester bond. This compound structure is known as polynucleotide. This alternating sugar-phosphate arrangement forms the primary structure of a DNA molecule. DNA presents then a secondary structure when it forms double-stranded DNA. It consists of two polynucleotides that are arranged such that nitrogenous bases of one polynucleotide are attached to the nitrogenous bases of another polynucleotide by hydrogen bonds. This base-to-base bonding follows a specific rule forming the Watson–Crick base pairs (bp): adenine interacts with thymine through two hydrogen bonds (A=T) and the guanine forms three hydrogen bounds with cytosine (G≡C). This ladder-like structure assumes a three-dimensional conformation, also known as tertiary structure. In 1952 Rosalind Franklin used the X-ray diffraction to capture images of DNA molecules and deduced its spiral shape. In 1953 Watson and Crick[35] argued that the DNA takes the form of a double helix. Different types of the double helices have been found in nature. Spatial arrangement of DNA can vary in handedness (right or left), length of the helix turn, number of base pairs per turn and difference in size between the major and minor grooves. B-DNA is a right-handed double helix with a constant diameter of 2 nm that has 10 bps per turns and where the distance between sequential base pairs is 0,34 nm. A-DNA is observable in dehydrating conditions, and is a right-handed double helix with 11 bps/turn and 0,21 $\frac{\text{nm}}{\text{bp}}$. Z-DNA is a more rare configuration where the helix is left-handed with 11 bps/turn and 0,38 $\frac{\text{nm}}{\text{bp}}$. In human body, if the DNA was a straight piece its length would be nearly two meters

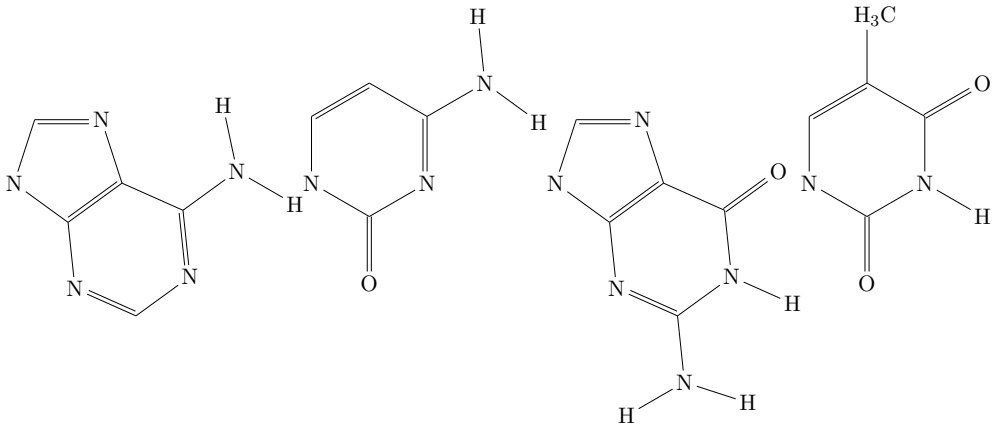

Figure 3.1
The structure of the nitrogenous bases.

long. In order to be contained in a cell (average dimension of 50 µm) of a prokaryotes organisms, or in the cell nucleus (average dimension of 6 µm) of a eukaryotes, the DNA has to be packed. The DNA packaging requires the double-strand to be tightly looped, coiled and folded. The negative charge of the DNA has to be compensated, for example by the positive charged amino acid residues in proteins like histone, and this reduces the intrinsic rigidity of DNA in order to compact it. On the other hand, during the process of replication, transcription and proofreading DNA has to be unwound. Therefore, it appears clear that the knowledge of the energy costs of these processes is important for a better comprehension of DNA formation and dissociation, and might be obtained by the determination of the elastic response of DNA under mechanical force action.

3.1 The DNA sequences

The DNA sequences used in this work are obtained from the so called lambda DNA (λ-DNA), a linear double strand 48502 base pairs DNA. Lambda is a Escherichia coli bacteriophage (bacterial virus) in which the genome is contained in the capsid. The molecule is multiplied (amplified) through the polymerase chain reaction (PCR) and with this process is possible to build different DNA with different lengths. However, after the PCR process the final sample could contain wrong-truncated DNA molecules and oligonucleotides with disincorporated bases, so a purification step is required to get the DNA with only the desired base-pair composition. To this aim, the agarose-gel electrophoretic technique was use, thus obtaining a separation of the different length populations. This method uses an electric field to move the molecules in a gel matrix: the net displacement is correlated to DNA length so that all the molecules having the same dimensions are gathered together. Once the portion of gel containing the DNA with the desired length has ben isolated, the DNA molecules are extracted by treating the gel with the QIAquick Gel Extraction kit.

Molecule	Contour length L_0
24 kbp	8160 nm
9 kbp	3060 nm
3,6 kbp	1224 nm

Table 3.1
Contour length of the molecules used in this work.

In particular, in this thesis work DNA molecules with three different length have been investigated and they are indicated by the number of their base pairs with the prefix kilo (k), 24 kbp, 9 kbp and 3,6 kbp. The so-called contour length L_0 of each molecule type can be calculated from the number of their base pairs multiply by the inter-nucleotides average distance that for the λ-DNA is $0{,}34\,\mathrm{nm\,bp^{-1}}$ as reported in Table 3.1. The physical and biological meaning of the parameter L_0 will be better described in the next section.

3.2 The DNA elastic model

Using the optical tweezer it is possible to stretch the DNA and record its mechanical response under an applied force. As a matter of fact, the DNA is bounded between two beads, one of which is kept fix while the other is moved by the optical trap: in this way it is possible to vary the distance between the beads, thus stretching the molecule and applying to it a known force. During this process the molecule experiences transitions across different conformational regimes (see Figure 3.2).

When it is not attached between the beads, DNA is in the so called *random coil* configuration. In this configuration the monomers are randomly oriented and realize a compact shape. With real polymer the subunits (the nucleotides) are not freely jointed because the interactions bind the flexibility of the chain; in this case an effective unit length can be used to describe the biological system. At lower force, less than 5 pN, DNA exhibits entropic response characteristic of the random coil. With force higher than 5 pN there is the enthalpic regime, where DNA extension stretches beyond its *contour length* L_0, which is the dimension of the molecule if the inter-nucleotides distance is constant. At sufficiently high forces (greater than 65 pN), the DNA transforms reversibly form the B-form to a new molecular state (called S-form, see Figure 3.3), presenting a transition called *over-stretching* where, at almost constant forces, the elongation reaches values up to 1,7 times the contour length. The molecular details of this state are still under debate[37–39]. The first interpretation was DNA adopts an unwound but base-paired structure, but recently the thermodynamics studies of the DNA suggests that the interaction between the bases gradually dissolves, even if a strand separation was not observed[40]. Above this region, molecule extension starts to increase again with the force. Investigations in this region is difficult due to the limits of the force range of the optical tweezer ($F_{\max} \sim 100\,\mathrm{pN}$), but also because at high force the streptavidin-biotin bond breaks and the whole stretching process has to start again from the beginning. For these reasons, other methods can be used in order to explore this regime, such as the an atomic force

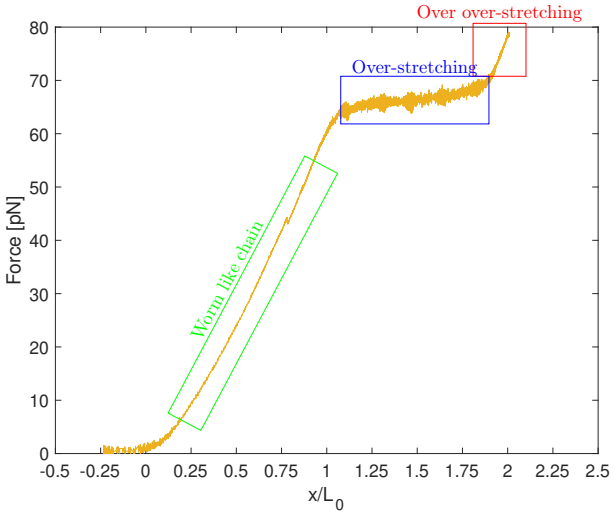

Figure 3.2
The response of double strand $3{,}6\,\mathrm{kbp}$ DNA under the action of a force. The molecule is well described by the worm-like-chain model for forces less than $50\,\mathrm{pN}$. Over this range the DNA increases its own length up to 70% of its contour length L_0. This region is called over-overstretching. Above the over-overstretching the extension of the molecule returns to be force dependent.

microscopy[41], although in this case a worse spatial and temporal resolution is achieved.

In a molecular physics framework, DNA can be theoretically described as the union of interacting monomers with specific degrees of freedom forming a precise configuration called polymeric chain. Given n+1 monomers $(A_0, \ldots, A_n)$, each of them separated by the next one by a fix distance r_i, the maximum physically possible extension of the polymeric chain is called contour length L_0 and it is equal to $L_0 = nr_i$. Another important parameter in describing the DNA polymeric chain is the persistence length L_p, which is the distance ove which DNA spontaneously bends due to thermal forces. In other words, L_p represents a characteristic length scale over which the vectors tangent to two base pair remain correlated and it is usually exploited to describe the "stiffness" or "rigidity" of a polymeric chain. Indeed, many biological systems have an intrinsic

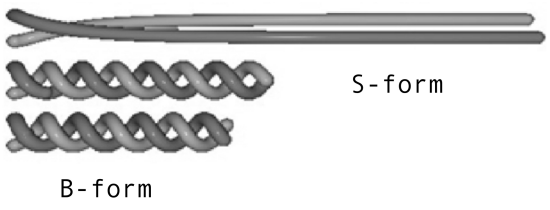

Figure 3.3
A schematic representation of the reversibly transformation of a DNA from its B-form, the usual configuration, to a new molecular state, called S-form, when a sufficiently high forces (greater than $65\,\mathrm{pN}$) stretches the molecule[36].

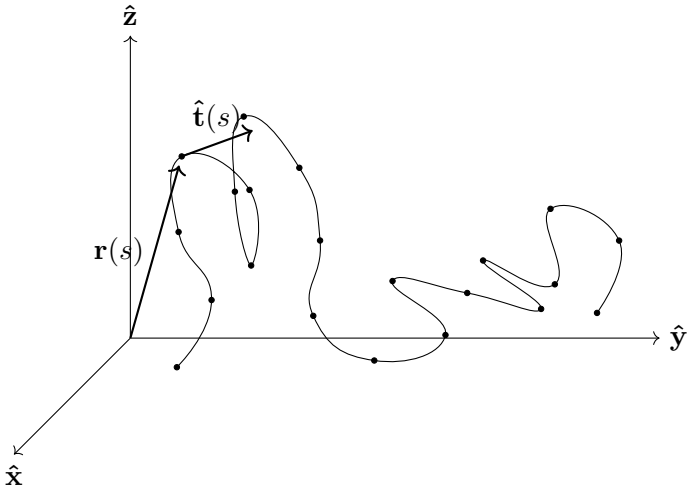

Figure 3.4
The DNA models like a stiff rod.

elasticity which forces them to remain rigid at small length scale even if they present a significant flexibility at longer scales; the persistence length is strictly connected to this phenomenon. In a double-stranded DNA $L_p \simeq 50\,\mathrm{nm}$ and involves about 150 bp, so it is possible to use continuum hypothesis and describe the molecule as an isotropic rod[42].

The behavior of the DNA in aqueous solutions is well described by the worm-like-chain (WLC), which assumes the DNA chain to be inextensible, with a linear bending energy and affected by thermal fluctuations. In this model[4, 43, 44] the double helix DNA is considered stiff, so the conformational fluctuations can be described with by a linearly elastic rod with a fixed contour length. Self-interactions or excluded volume effects are negligible under most experimental conditions and perturbations form the equilibrium can be described in terms of energy costs.

The DNA conformations can be described by a curve in space $\mathbf{r}(s)$ where s is the arc length and $\hat{\mathbf{t}}(s)$ is the unit tangent vector at location s along the polymer (see Figure 3.4). The bending energy per length is equal to:

$$\frac{\mathrm{d}E_b}{\mathrm{d}s} = \frac{1}{2}A\left|\frac{\mathrm{d}\hat{\mathbf{t}}(s)}{\mathrm{d}s}\right|^2 = \frac{1}{2}A\kappa^2$$

where κ is the reciprocal of bending radius, also called curvature. The proportional term $A = (230 \pm 20)\,\mathrm{pN\,nm^2}$[4] is linked with the persistence length L_p, the characteristic distance over which the correlation of the tangent vector $\hat{\mathbf{t}}(s) = \partial\mathbf{r}(s)/\partial s$ die off, i.e. the distance over which a bend can be made with a cost of k_BT. This relation is $A = k_BTL_p$. Therefore, when a force F is applied to the DNA molecule for stretching it, the total energy of the system is given by

$$E = \int_0^{L_0}\left(\frac{A}{2}\left|\frac{\mathrm{d}\hat{\mathbf{t}}(s)}{\mathrm{d}s}\right|^2 - F\cos[\phi(s)]\right)\,\mathrm{d}s$$

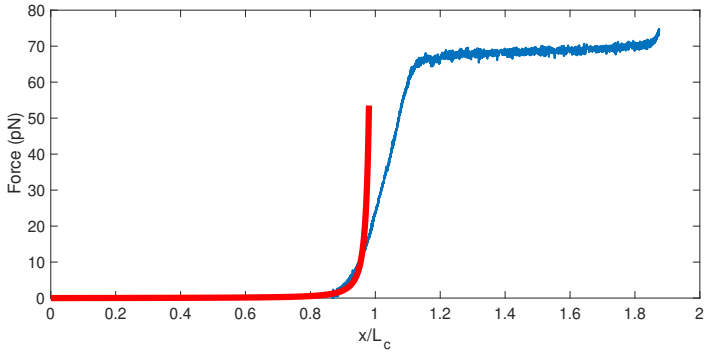

Figure 3.5
The interpolation of the a force-extension curve with the Bustamante's approximation formula.

where the first term represents the resistance of the chain to the bending, while the second term is the work done by the force for aligning the molecule, being $\phi(s)$ is the angle formed between the force and the $\hat{\mathbf{t}}(s)$.

The previous formula can be numerically solved, even if an analytical solution doesn't exist. However, the formula proposed by Bustamante and Mark et Siggia[44] is usually employed, which connects the applied force with the measured DNA extension z

$$F = \frac{k_B T}{L_p}\left[\frac{1}{4(1-z/L_0)^2} - \frac{1}{4} + \frac{z}{L_0}\right] \tag{3.1}$$

Even possible correction of this formula exists (for example by adding a seventh-order polynomial in z/L_0) this result well fits the experimental data below 30 pN (see Figure 3.5).

The chiral nature of DNA and the experimental observations of the changing of the contour length even before the over-stretching region requires an extension of the previous model[4]. Twisting and stretching have to be taken in account, above all at high applied forces.

When intrinsic stretching is considered, the arc length s must be replaced with an internal coordinate ζ, define as $\mathrm{d}\zeta = \mathrm{d}s/v = \mathrm{d}s/(1+u)$, where u is the axial strain. This new coordinate can be considered as arc length in the absence of thermal fluctuations or chemical distance along the chain. The tangent vector, along the curve, is given by:

$$\frac{\mathrm{d}\mathbf{r}(\zeta)}{\mathrm{d}\zeta} = v\hat{\mathbf{t}}$$

Small extension costs an energy equal to

$$\frac{\mathrm{d}E_s}{\mathrm{d}\zeta} = \frac{1}{2}Su^2$$

where S is the stretch rigidity (or stretch modulus) and it usually assumes values around 1000 pN[4].

Twisting is described by the angle per arc length that the base pairs rotate around $\hat{\mathbf{t}}$. An unperturbed DNA has a pitch of helix of 3,5 nm (10,5 bp) and thus a twist rate of

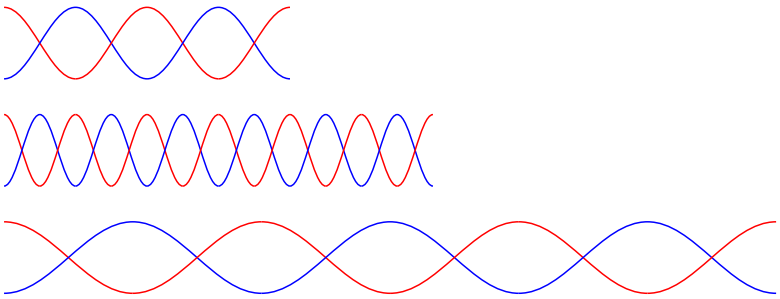

Figure 3.6
Schematic representation of double-stranded DNA under stretching deformation (above). At low forces ($< 35\,\mathrm{pN}$) is expected that the molecule overwinds (center) thus reducing its pith (distance to complete one turn) while at high forces it unwinds (below).

1,8 $\frac{\mathrm{rad}}{\mathrm{nm}}$. Deviation Ω, from the twist rate, costs an elastic energy proportional to:

$$\frac{\mathrm{d}E_t}{\mathrm{d}\zeta} = \frac{1}{2}C\Omega^2$$

where $C = (460 \pm 20)\,\mathrm{pN\,nm^2}$[4] is the twist rigidity (or twist modulus) and it is linked to the persistence length for twist fluctuations ($L_\theta = C/k_BT$).

Although there are no evidences for coupled twisting and bending, some experiments shed light on twist-stretching coupling[4, 39, 45]. This energy per length term is proportional to a factor g. The studies of the transition between the B-form to the overstretching configuration of the DNA suggests a positive value of g ($(200 \pm 100)\,\mathrm{pN\,nm}$) meaning that DNA unwinds itself when stretched. On the contrary, further experimental results and simulations suggest that the molecule overwinds when stretched in a force range below $35\,\mathrm{pN}$ ($g = -(90 \pm 20)\,\mathrm{pN\,nm}$) and unwinds when stretched with an higher force (see Figure 3.6). Therefore, not only the value of g is controversial, but also its sign. The energetic contribution of the twist-stretching coupling is given by:

$$\frac{\mathrm{d}E_{ts}}{\mathrm{d}\zeta} = gu\Omega$$

In summary the total energy, for a DNA molecule under the action of a force F is given by:

$$E = \int_0^{L_0} \left[\frac{A}{2}\left(v\frac{\mathrm{d}\hat{\mathbf{t}}}{\mathrm{d}\zeta}\right)^2 + \frac{C}{2}\Omega^2 + \frac{S}{2}u^2 + gu\Omega - Fv\cos[\theta(s)] \right] \mathrm{d}\zeta \tag{3.2}$$

Chapter 4

Force-spectroscopy experiments on single molecules

Understanding the DNA elasticity properties is the cornerstone for a better comprehension of its biological properties and functionalities. Nowadays three main questions are still under debate, that are the behavior of the DNA in the over-stretching regime, its elastic response at forces higher than 65 pN to 67 pN and the role played by the coupling of the stretch and twist of the molecule. Concerning this last aspect, the corresponding energetic contribution is proportional to the factor g, which has been recently investigated by means of molecular dynamics simulations[2] and magnetic tweezers[3, 4]. The result widely shared is that g seems to change its sign with the force, in particular it is negative for forces below 30 pN, an so the DNA overwinds, whereas above this value, g becomes positive and the molecule unwinds when stretched. However, these results partially contradict previous investigations and a clear and widely-accepted theoretical model explaining this effect is still lacking.

In this chapter it will be presented a new approach which tries to shed light on the mentioned problems. The optical tweezers technique was used to investigate the motion of a bead in the optical trap when it is linked to a single DNA molecule. The idea is that of looking at the force power spectrum of the bead in order to infer some information about the elastic properties of the biological system. The results here presented, provide a qualitative description of the phenomena, highlighting the role played by the different elastic contributions in the frame of a first tentative theoretical model.

4.1 High frequency force-spectroscopy

4.1.1 Theoretical model

As described earlier, the DNA is stretched by modifying the distance between two beads to which the molecule is tethered. One bead is kept at fix position through a micro pipette, and the other is moved by changing the position of the optical trap. Therefore a known force is applied to DNA and in principle its reaction to this external force can be studied by monitoring the movement of the bead in the optical trap. As a matter of fact, the movement of the trapped bead is affected not only by the force exerted by the optical

trap itself, but also by the presence of the linked DNA chain. Any variation in the force F experienced by the bead is recorded by the Position-Sensitive-Detectors (as explained in chapter 2) and its power spectrum $\mathbb{P}_F(\omega)$ can be derived as the autocorrelation of the measured force:

$$\mathbb{P}_{F_y}(\omega) = \langle |\tilde{F}(\omega)|^2 \rangle$$

Since the optical trap can be compared with a simple spring which follows Hooke's law, the force is related to the bead position as

$$F = \kappa(x - x_0)$$

from which it follows:

$$\mathbb{P}_F(\omega) = \kappa^2 \mathbb{P}_x(\omega)$$

where $\mathbb{P}_x(\omega)$ is the power spectrum of the bead position, defined as

$$\mathbb{P}_x(\omega) = \langle |\tilde{x}(\omega)|^2 \rangle$$

At this point, it is possible to remember that the DNA molecule can be modeled as an extensible isotropic rod, as reported in the previous chapter, so that the total energy of the DNA/bead system is:

$$E(x, \theta, x_0) = \frac{S}{2}\frac{x^2}{L} + \frac{C}{2}\frac{\theta^2}{L} + g\frac{x\theta}{L} + \frac{\kappa}{2}(x - x_0)^2 \tag{4.1}$$

where S,C and g are the stretch modulus, the twist modulus and the twist-stretch coupling parameter, respectively; κ is the stiffness of the trap, x is the variation of DNA length (that is also the variation of the bead position) with respect to the starting reference position x_0; θ is the additional twist to the normal helical twist and L is the contour length. As first approximation the bending contribution has been neglected, the range of forces investigated in this work well above 20 pN, where usually the stretch and twist contributions dominate.

In the model proposed by M. Baiesi and F. Seno[46], the bead is assumed to have a radius a ($a = 1{,}5\,\mu\text{m}$) and to be immersed in a thermal bath at temperature T with viscosity η. The overdamped stochastic equations are as:

$$\begin{aligned} \frac{\partial x}{\partial t} &= \mu_x \left(-\frac{\partial E}{\partial x}\right) + \sqrt{2k_B T \mu_x}\xi_x \qquad (4.2) \\ &= -\mu_x \left(\frac{S}{L} + \kappa\right) x - \mu_x \frac{g}{L}\theta + \kappa x_0 + \sqrt{2k_B T \mu_x}\xi_x \\ \frac{\partial x}{\partial \theta} &= \mu_\theta \left(-\frac{\partial E}{\partial \theta}\right) + \sqrt{2k_B T \mu_\theta}\xi_\theta \qquad (4.3) \\ &= -\mu_\theta \frac{C}{L}\theta - \mu_\theta \frac{g}{L} x + \sqrt{2k_B T \mu_\theta}\xi_\theta \end{aligned}$$

where the mobilities μ_x and μ_θ are defined:

$$\mu_x = \frac{1}{6\pi\eta a}$$
$$\mu_\theta = \frac{1}{6\eta 4/3\pi a^3}$$

and they are relative to a spherical body, being the DNA contribution negligible because it is much smaller that the bead.

By using the previous formulae, the power spectrum of the force can be rewritten as:

$$\mathbb{P}_F(\omega) = \frac{\kappa^2\alpha\left[1+\left(\frac{\omega}{\beta}\right)^2\right]}{\gamma^4+\delta^2\omega^2+\omega^4} \tag{4.4}$$

with:

$$\alpha = (2k_BT)\mu_x\mu_\theta\left[\left(\mu_\theta\frac{C^2}{L^2}\right)+\left(\mu_x\frac{g^2}{L^2}\right)\right] \tag{4.5}$$

$$\beta = \sqrt{\mu_\theta\left[\left(\mu_\theta\frac{C^2}{L^2}\right)+\left(\mu_x\frac{g^2}{L^2}\right)\right]} \tag{4.6}$$

$$\gamma = \sqrt{\left|\mu_x\mu_\theta\left[\left(\frac{g}{L}\right)^2-\frac{C}{L}\left(\frac{S}{L}+\kappa\right)\right]\right|} \tag{4.7}$$

$$\delta = \sqrt{\left[\mu_x^2\left(\frac{S}{L}+\kappa\right)^2+2\mu_x\mu_\theta\left(\frac{g}{L}\right)^2+\left(\mu_\theta\frac{C}{L}\right)^2\right]} \tag{4.8}$$

where $\delta/(2\pi)$ is the corner frequency.

The formula of the power spectrum can be simplify for high frequencies, such as $f \geq 1\,\text{kHz}$:

$$\mathbb{P}_F(\omega) \simeq \frac{\kappa^2\alpha/\beta}{\delta^2+\omega^2} = \frac{2k_BT\mu_x}{\delta^2+\omega^2}$$

so it is possible to fit the data, near the corner frequency, with the function:

$$P(\nu) = \frac{A}{\nu_c^2+\nu^2} \tag{4.9}$$

where ν is the frequency ($\omega = 2\pi\nu$). In this approximation the amplitude A is independent of any elastic parameters and its value is determined only by the temperature T of the system and the mobility μ_x of the bead. However, it must be kept in mind that the last formula is valid only under the assumption that $\omega \gg \beta$ which depends on the value of g. As a matter of fact, in Figure 4.1, it is possible to notice as A remains constant only in a well defined range of frequencies, whose limits vary with g (see Figure 4.1b). Moreover, it is worth mentioning as g also affects the parameter α (see Figure 4.1a), which becomes relevant al lower frequencies, so that the amplitude of the force power spectrum is not more constant and it strongly changes with ω.

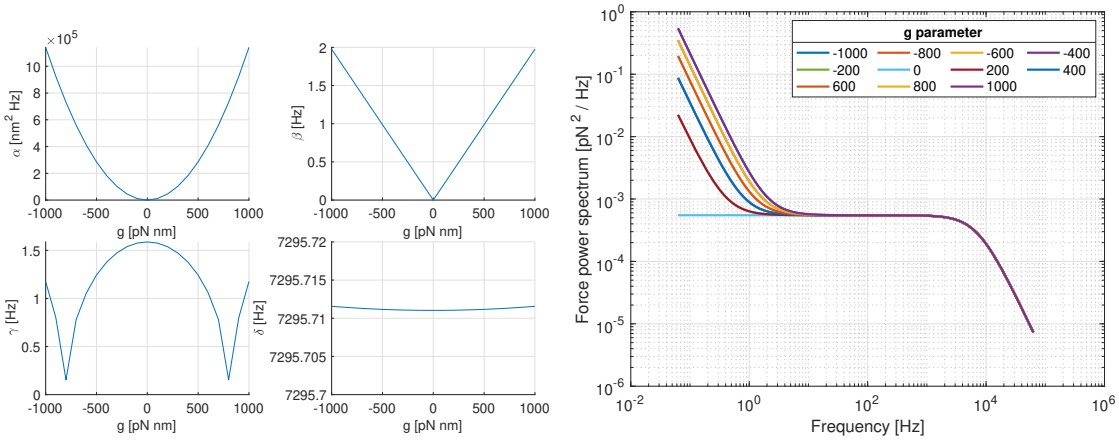

Figure 4.1
In (a) are represented the parameters of the force power spectrum in function of the twist-stretch coupling g. The power spectrum function in (b) is pictured changing the value of g for a 24 kbp DNA. The values used for the other terms are reported in table Table 4.1.

4.1.2 Experimental data acquisition

The first step of the experimental procedure is tethering the molecule. As already explained in the previous chapter, the DNA molecules have been already attached to a Antidigoxigenin covered bead (AD bead) by performing an incubation protocol. Streptavidin bead (SA bead) is introduced in the microfluidic chamber and it is caught by suction of micro-pipette, while the second bead, the one functionalized with Antidigoxigenin, is trapped by optical tweezer. Moving these beads closer to each other, Streptavidine could bind to the Biotine on the free side of random coil configuration DNA. The single molecule can not be seen by the optical tweezer imaging system (see Figure 4.2), however molecular density was properly tuned during the incubation step in order to have some molecules per bead. DNA catching is verified if the optical tweezer PSD measure a force when the two beads are moved away beyond the contour length of the investigated molecule. Usually it is necessary repeat this procedure several times, until one and only one molecule is tethered between the two polistirene beads. As a matter of fact, it often happens that two or more molecules are linked to the beads, so that the system should be brought to higher forces till only one bond endures.

DNA is stretched when the beads are moved away along the $\hat{\mathbf{y}}$ axis (i.e. vertical direction), and the total force acting on the AD bead can be measured in real time by optical tweezer software. By adjusting the positions of the beads, force components, other than F_y, are set to zero so that a well-known force is applied to the system along an unidimensional direction. The force signal of the system ($\mathbb{S}_f(F_y)$) is recorded with sample rate of $f = 50\,\text{kHz}$ for $t = 5\,\text{s}$, while the force applied to the bead is kept constant. The procedure is repeated changing the force from 0 to 80 pN to get information along all the different different regimes of the DNA elongation (worm like chain regime, overstretching, above over stretch region). Unfortunately, often the Streptavidin-Biotin bond

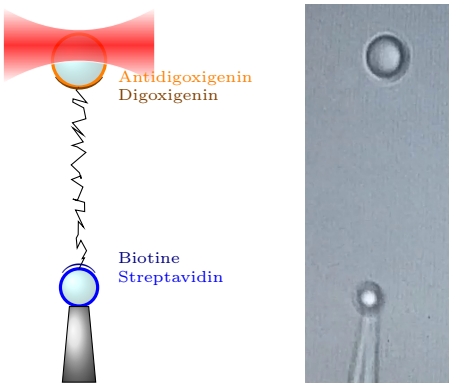

Figure 4.2
On the right, it is pictured what can be seen on the optical tweezer screen. Between the two beads there is a single molecule DNA, but the imaging system can not resolve it. On the left there is a schematic representation of a typical force spectroscopy experiment.

Parameter	Value
S	$1100\,\mathrm{pN}$
C	$303\,\mathrm{pN\,nm^2}$
κ	$0{,}1\,\mathrm{pN\,nm^{-1}}$
γ	$1{,}002 \times 10^{-9}\,\mathrm{pN\,nm^{-2}}$
a	$1{,}5 \times 10^{3}\,\mathrm{nm}$
μ_x	$3{,}53 \times 10^{4}\,\mathrm{nm\,pN^{-1}\,s^{-1}}$
μ_θ	$1{,}18 \times 10^{-4}\,\mathrm{nm^{-1}\,pN^{-1}\,s^{-1}}$

Table 4.1
The value used for estimate the parameters used in the power spectrum formula[4, 46].

breaks during the measurement, in particular at forces above 40 pN, so that the whole procedure has to start again from the beginning and a new molecule has to be caught.

The force spectra are then elaborated with MATLAB script. First, the raw voltage signal (Figure 4.3a), acquired by the high-frequency-board, is converted into a force signal (Figure 4.3b) by means of the calibration presented in section 2.6. Then the force power spectrum (Figure 4.3c) was calculated with ad-hoc MATLAB scripts and, for sake of simplicity during the subsequent analysis, the spectrum was subdivided into frequency-windows with fixed-width. Finally, the averaged data corresponding to each frequency window were reported in a log-log scale (Figure 4.3d). This data are then interpolated with the lorentzian function given by equation (4.9) to obtain the amplitude A and the corner frequency ν_c (see Figure 4.3).

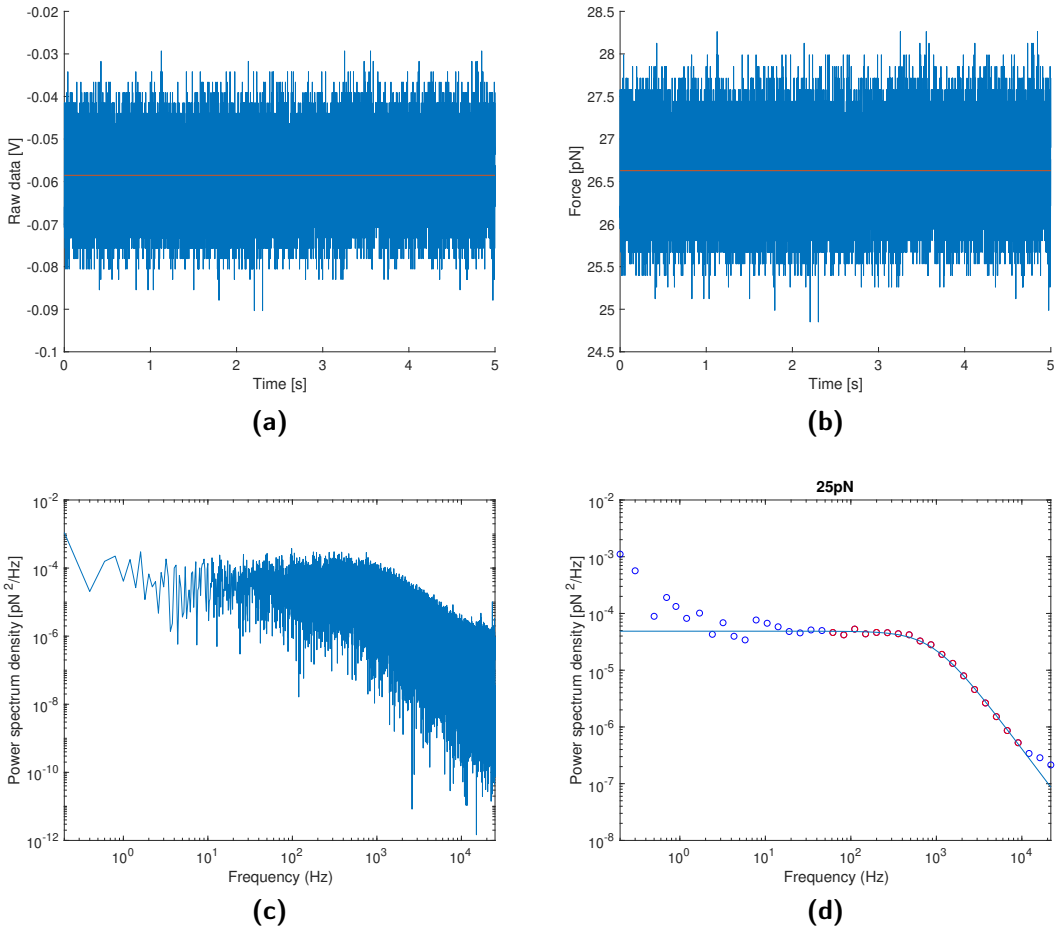

Figure 4.3
The raw voltage signal (a), is converted as force data (b). Those are elaborated in order to get the force power spectrum (c) that is fitted with the lorentzian function(d).

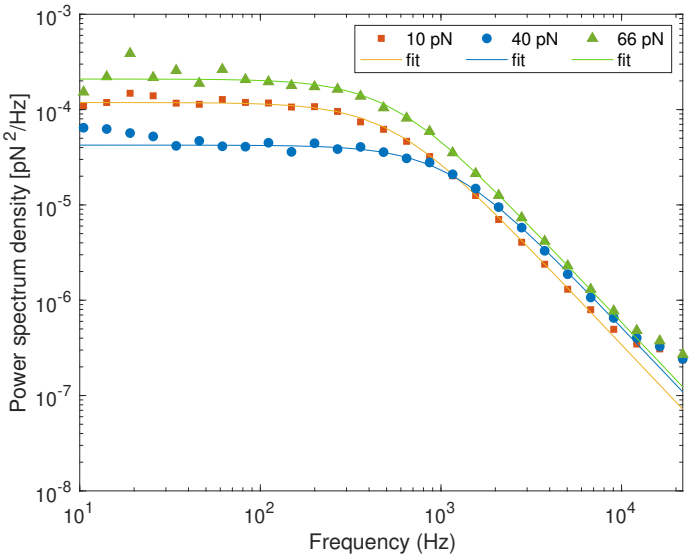

Figure 4.4
A closer look, in the high frequency region, of three power spectra of a molecule that was pulled by a force of 10 pN, 40 pN and 66 pN.

10 pN		40 pN		66 pN	
A [pN Hz]	30 ± 2	A [pN Hz]	52 ± 3	A [pN Hz]	58 ± 3
ν_c [Hz]	537 ± 22	ν_c [Hz]	1109 ± 40	ν_c [Hz]	530 ± 26

Table 4.2
The fit parameters of the the lorentzian function (4.9) used to fit the power spectra of Figure 4.4.

4.2 Results and discussion

As first test, the 24 kbp DNA molecule was considered, since it is a well-known molecule in the field of optical-tweezers and it is quite stable and resistant also at high pulling forces. In Figure 4.4 the force power spectra obtained for the same molecule at 10 pN, 40 pN and 66 pN (over-stretching region) are reported and the corresponding fits are shown. In Table 4.2 are reported the fit parameters and, as it is possible to notice, both the amplitude and the corner frequency of the force power spectrum change with force, suggesting that a variation of the elastic constants of the system is occurring as the force applied to the polymeric chain is increased. Thanks to the high resistance of this biological system, it was possible to measure the power spectra of more than 40 molecules of lambda DNA, from 0 pN to almost 90 pN, with mean force-step of 5 pN. The amplitude and the corner frequency of each spectrum were calculated and the obtained values are reported in Figure 4.5 and Figure 4.6, where only the more relevant molecules are shown for sake of clarity.

4.2.1 Molecule 24 kbp

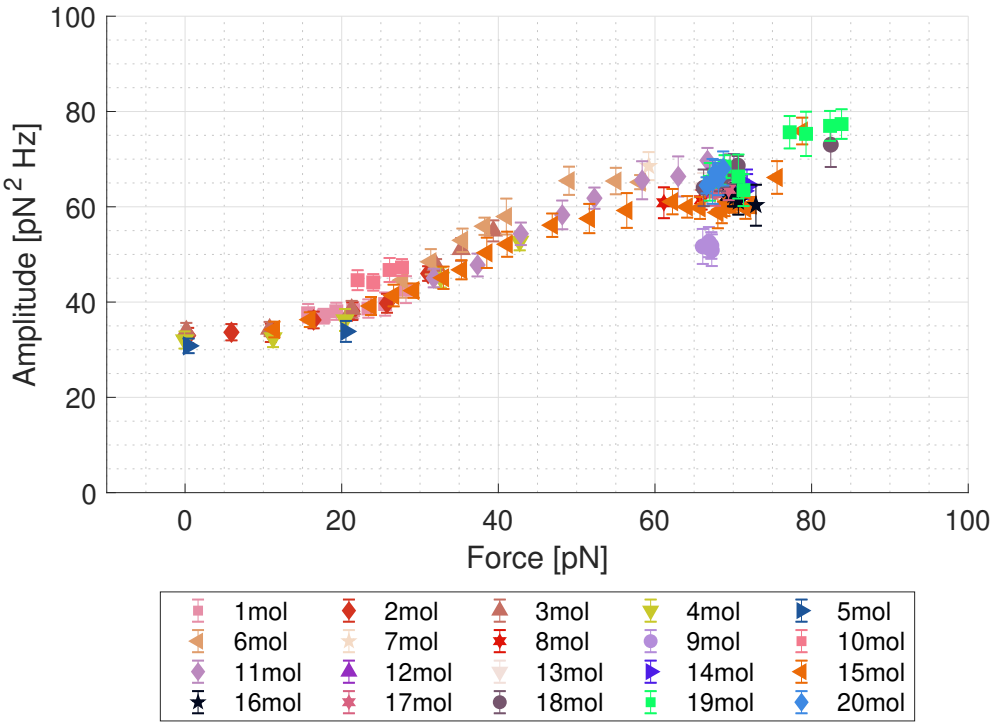

Figure 4.5

Amplitude The graph Figure 4.5 report the amplitudes of the lorentzian fit in function of the force. At lower forces, such as $F < 15\,\text{pN}$, the amplitude doesn't vary significantly with the force, confirming the results already found in another work[47]. The same trend seems is also observed in the over-stretch region, between 65 pN to 75 pN. Contrary of expectations, in the other force ranges the amplitude growths with the force. The approximation $\omega \gg \beta$, that was introduced to simplify the power spectrum formula, seems not be satisfied and other terms have to take in account to understand the variation of the power spectrum amplitude. As a matter of fact if β was comparable with ω, the role of g and C could not be neglected.

Even if the twisting contribution could be probably neglected since in equation (4.6) $\mu_\theta \ll \mu_x$, however a relevant increase of g (above 500 pN nm) with respect to the values reported in literature for lower forces could explain the observed trend of A. In this case, A would be dependent on g^2 (see equation (4.5)) and therefore any informations on the sign of the g parameter couldn't be derived. Anyway, it would be clear the dependence of g on the force, as suggested by other works[2–4, 39]. In connection with this, it is worth noting as the most relevant variation of A occurs between 20 pN and 50 pN, that is the force range where a change from the overwound to the unwound DNA configuration is expected. Clearer information could be derived by investigating low-frequency regions where the contribution of g is predicted to be more pronounced (stronger).

Finally, it is possible to notice as some molecules present values of the amplitude that

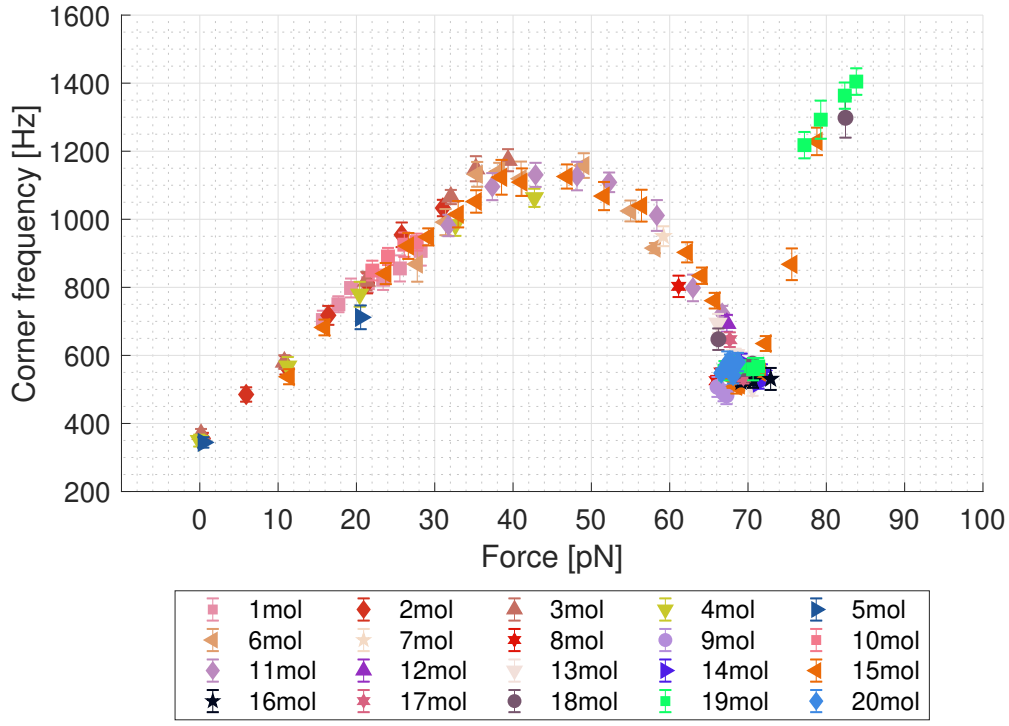

Figure 4.6

slightly differ from the other ones (as the molecules n° 6 and n° 10): this is probably due to a little difference in the molecules length, as it will be clarified in the next sections. Indeed, the preparation procedure of the DNA molecules (see section 3.1) requires a post-PCR purification step, which could results in a biological sample with molecules having slightly different lengths.

Corner frequency From the graph Figure 4.6 it can be seen a significant and more clear variation of the values of the corner frequency with the force. The curve of the corner frequency start to increase after a first minimum and it reaches its local maximum near 35 pN; then it starts to decrease until another local minimum in the over-stretching region is reached. After that it start rising again above this force range. In the frame of the model presented in section 4.1.1 (see (4.7)) δ is dependent from S/L which represents the stiffness of the DNA divided by its contour length and the twist-stretch coupling parameter g. However, also at very high g values (above 1000 pN nm) the contribution of g would be very weak being modulated by the factor μ_θ, which is 8 orders of magnitude lower than μ_x. Therefore, as first approximation, δ can be considered to be affected only by S/L:

$$\delta \simeq \left| \mu_x \left(\frac{S}{L} + \kappa \right) \right|$$

Being the molecule length L a constant for the same DNA population, the variation of the corner frequency is directly connected to a change in the values of the stretch rigidity

parameter S. Increasing and decreasing of the corner frequency could be interpreted as a DNA molecule that became more stiff until $F \simeq 40\,\mathrm{pN}$ was reached. After that it became more prone to stretching. In literature the value $F = 35\,\mathrm{pN}$ is reported as the limit in which g changes it sign and DNA changes its behavior from overwinding to unwinding when it is stretched, therefore, form reported data it seems than a change in the DNA configuration is stringily connected also to a change in its stretch-rigidity.

4.2.2 Molecule 3.6 kbp

To verify if the obtained results have a general validity and clarify the possible role played by the DNA length, the same experimental investigation was performed also on DNA chain with different length, that is 3,6 kbp and 9 kbp.

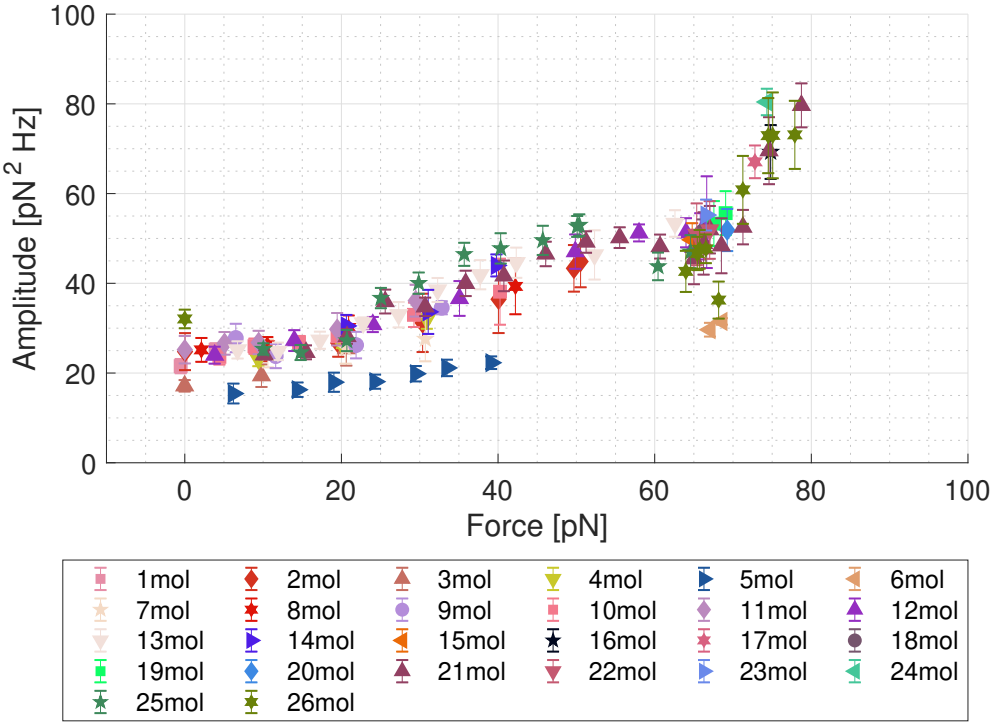

Figure 4.7

The same behaviors described previously, for the 24 kbp-long molecules, can be found also in a shorter molecules composed of 3,6 kbp. The amplitude is once again constant at low forces (< 15 pN) and in the over-stretching region, as it is possible to observe in Figure 4.7. Moreover, as for the 24 kbp DNA the amplitude significantly increases between 20 pN and 50 pN and above the over-stretching regime.

In the corner frequency graph (Figure 4.8) the general behaviors of the data are the same of the 24 kbp DNA, except for the presence of a second curve above the most populated one. This was verified to be linked with a mixture of molecular populations of difference length. In particular, the nature of the second population was investigated by observing the presence of second population was verify by observing the length of the plateaux L_{plateaux} of some molecules from which it was possible to deduce the contour length L_0. As a matter of fact, ita has been already widely demonstrated that the over-stretching region corresponds to a regime of the double strand DNA molecule were the polymeric chain increase its length of about 70% beyond its contour length L_0 without requiring a significant increase of the pulling force. Therefore in the over-stretching region the plateaux length is expected to be equal to $0{,}7 \cdot L_0$, that is $L_{\text{plateaux}} = 900$ nm for the 3,6 kbp DNA. The same reasoning applies for the molecules presenting a corner

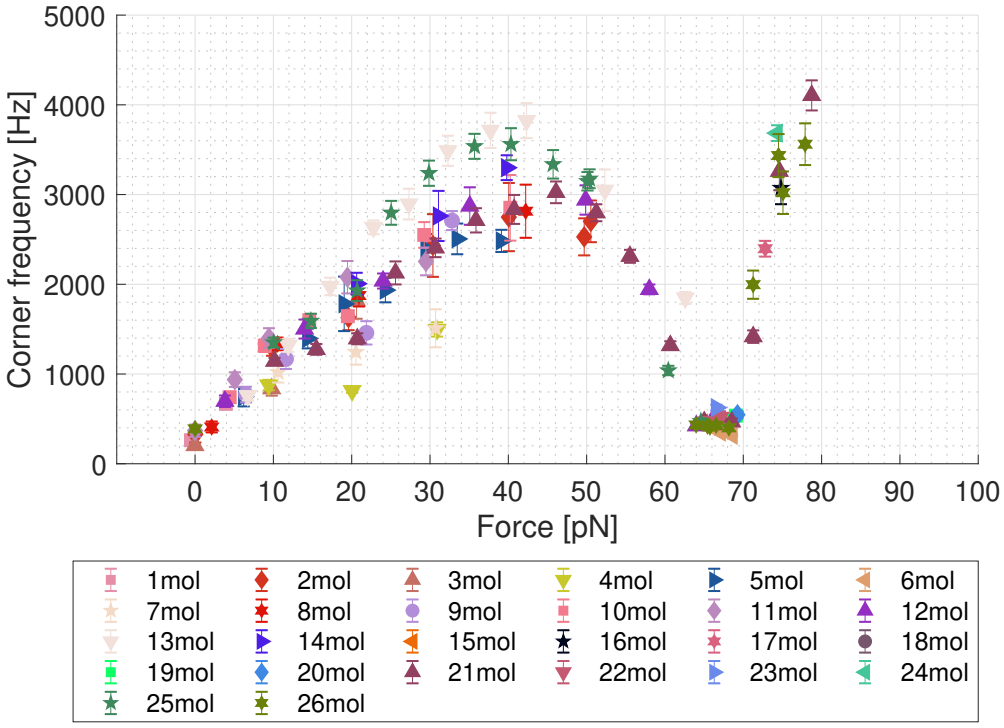

Figure 4.8

frequency value slightly below the most populated curve. In this case it was measure a length of the plateaux of almost 1100 nm, corresponding to molecules with a contour length around 5 kbp. As explained before, this is due to some incorrect steps in the purification procedure or PCR process. Anyway this problem has mainly affected the 3,6 kbp DNA samples, whereas in the 24 kbp and 9 kbp populations the incident rate of this issue was below 3%.

4.2.3 Molecule 9 kbp

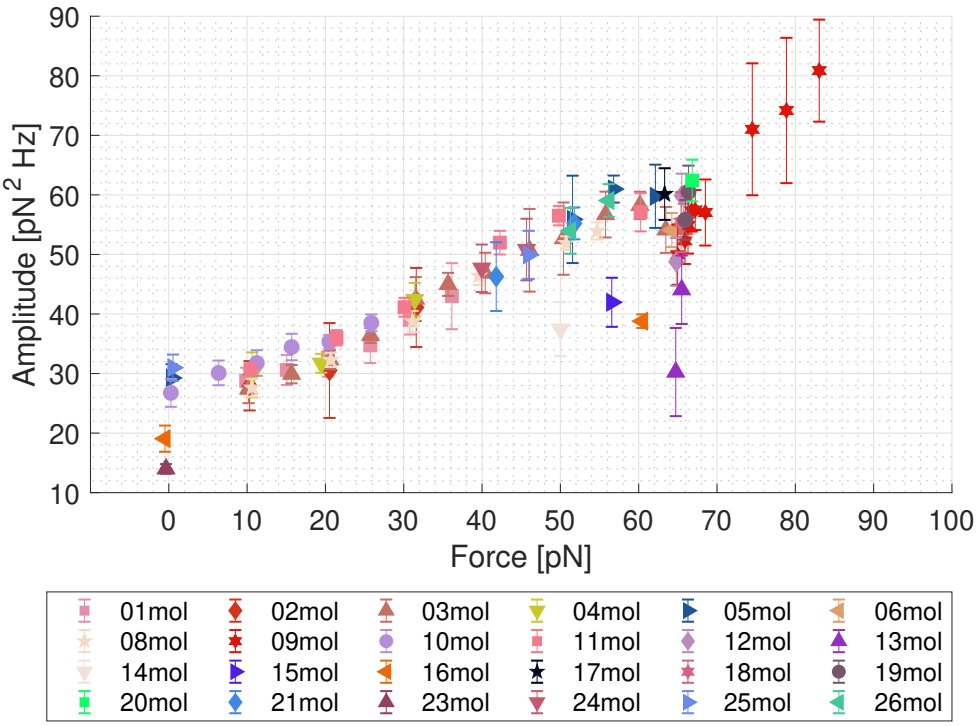

Figure 4.9

The last molecule, investigated in this thesis work, was a 9 kbp-long DNA chain. Results are shown in the following graphs (Figure 4.9 and Figure 4.10) in which it can be seen the same previously discussed behaviors.

During the experiments it was clear that both 9 kbp-long molecules and 3,6 kbp ones were less resistant than the 24 kbp DNA. It was quite hard to measure the power spectrum at forces above the over-stretching regime. Anyway, also in this case it appears clear that the force range around 30 pN to 40 pN is critical for the elastic behavior of the molecule, a result which is confirmed by the significant change in the stretch rigidity modulus and twist-stretch coupling parameter.

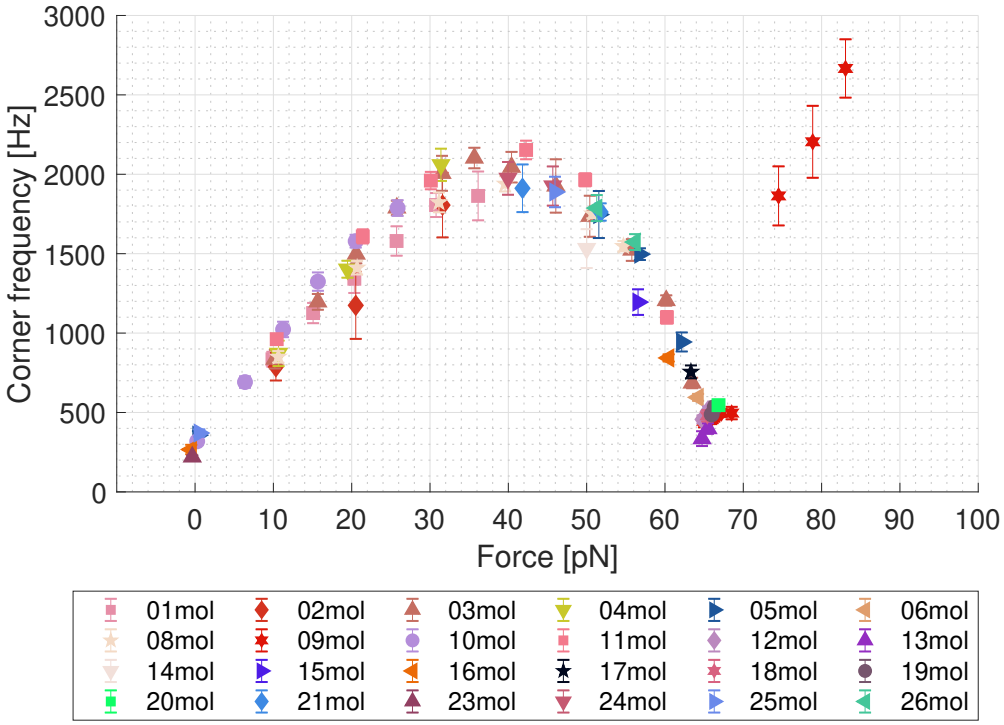
Corner frequency [Hz]
3000
2500
2000
1500
1000
500
0
0
10
20
30
40
50
60
70
80
90
100
Force [pN]
01mol
02mol
03mol
04mol
05mol
06mol
08mol
09mol
10mol
11mol
12mol
13mol
14mol
15mol
16mol
17mol
18mol
19mol
20mol
21mol
23mol
24mol
25mol
26mol

Figure 4.10

4.2.4 Comparison between molecules

A final comparison between the different investigated molecules is mandatory to obtain information about the dependence on the length of the elastic parameters of DNA.

The amplitude of the power spectrum increases clearly with the length L of the polymeric chain (see Figure 4.11). If a close link between variation of A with g would be confirmed by analyzing the low-frequency region of the spectra, it would results that the twist-stretch coupling depends on the length of the molecule considered, an unprecedented result.

Also the corner frequency changes with the length (see Figure 4.12). Higher corner frequencies can be interpreted as more stiff molecules and it seems to increase as the molecule length is shorten, getting a local maximum near 35 pN. Moreover, the corner frequency apparently increases with the force also above the over-stretching, but it is difficult to carry out measurements in this region because the bonds between SA beads and DNA are more fragile. At first approximation, corner frequency is proportional to S/L but from the Figure 4.12 the single contribution of these two factors can not be discriminated. In order to highlight the contribution of S, it can be directly calculated as

$$S = \left(\frac{\delta}{\mu_x} - \kappa \right) L_0$$

and it can be reported in function of the force and for different molecular lengths (see Figure 4.13). As it is possible to notice in the graph, the stretch rigidity depends on the molecule length; in particular, the maximum value of S for the 3,6 kbp is almost half of the corresponding value for the 24 kbp DNA. As a matter of fact, for the 24 kbp DNA, the stretch modulus is $S = (1186 \pm 79)$ pN which is compatible with $S = (1100 \pm 200)$ pN derived by J. Gore et al. in[4].

Finally, it should be mentioned the fact that the corner frequency and, as a consequence, the stretch modulus S, recovers the starting value measure at 0 pN when the over-stretching regime is reached. This means that at those forces the polymeric chain returns to be more easily stretched as at very low forces, and this is confirmed by the fact that in the over-stretching region it is possible to significantly elongate the DNA without increasing the applied force.

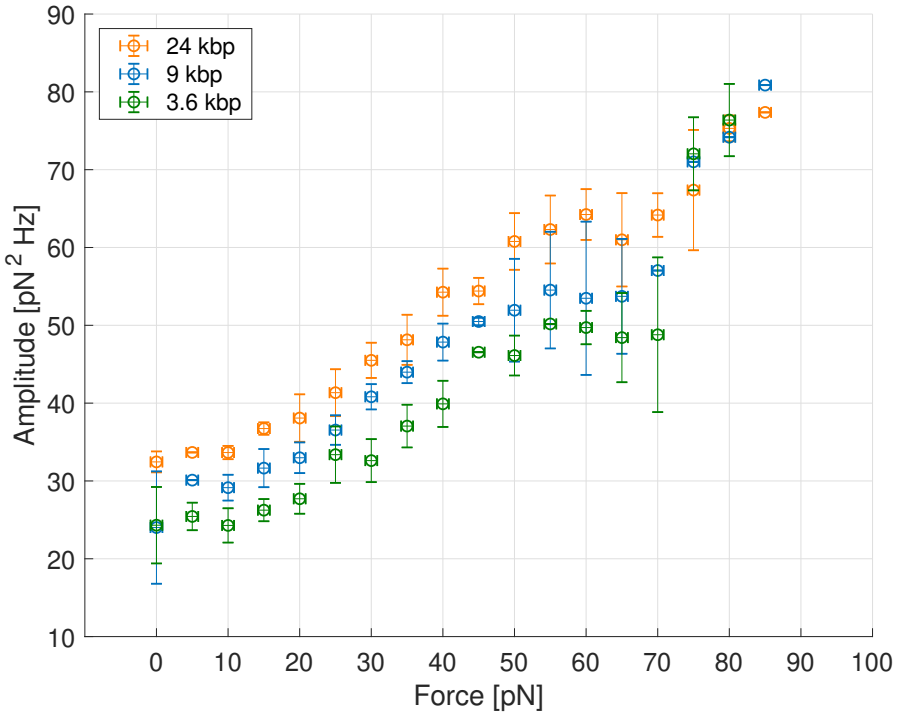

Figure 4.11

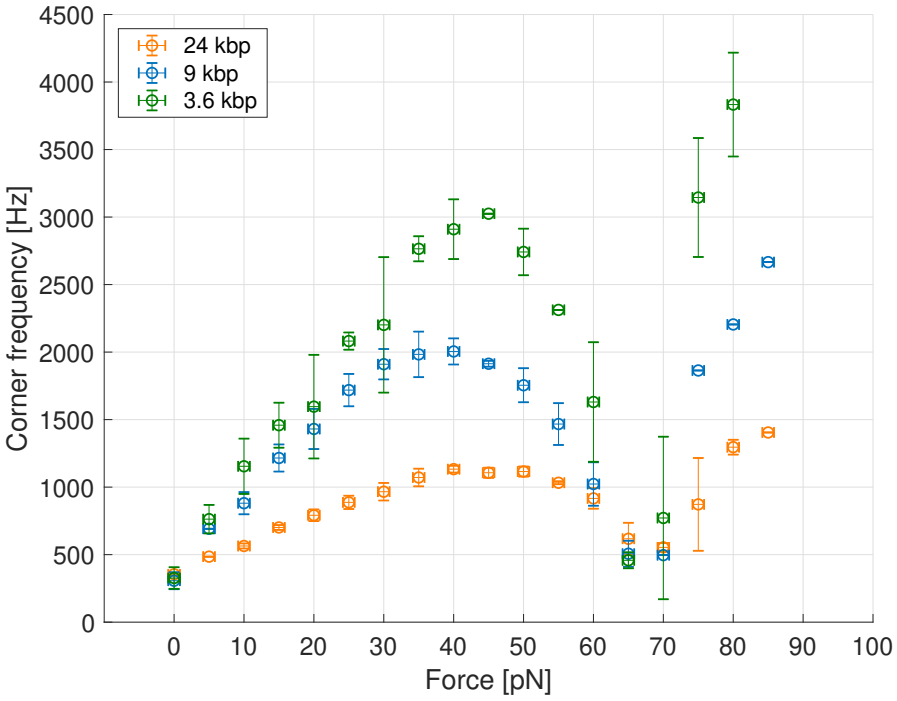

Figure 4.12

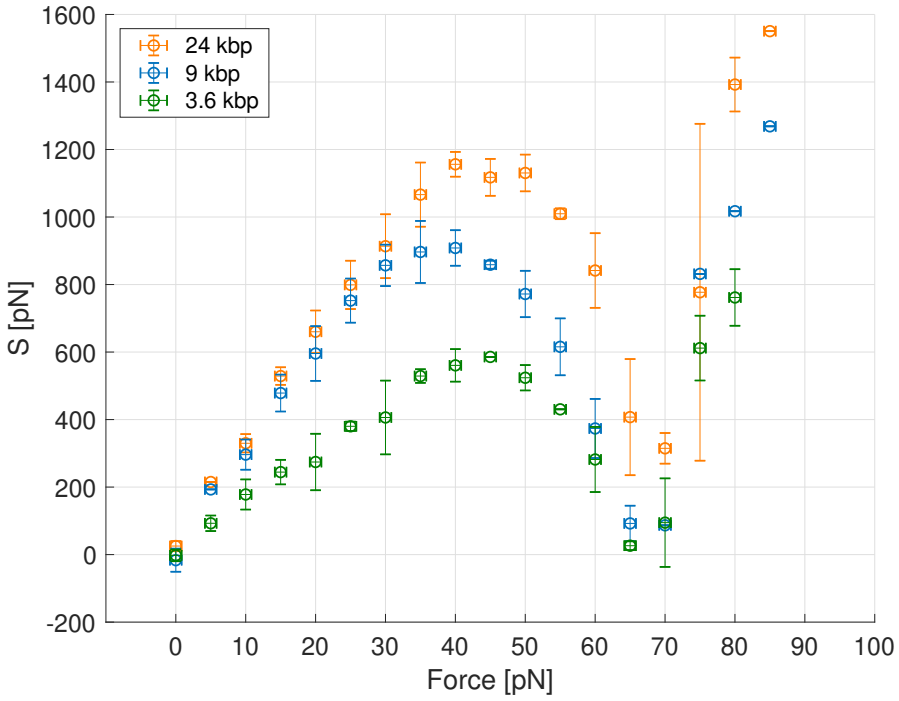
24 kbp
9 kbp
3.6 kbp
S [pN]
Force [pN]
1600
1400
1200
1000
800
600
400
200
0
-200
0
10
20
30
40
50
60
70
80
90
100

Figure 4.13

Conclusions and future works

In this thesis work the elastic response of double-stranded DNA molecules has been investigated by means of high-frequency force spectroscopy with optical tweezers. The main goal was that of demonstrating the feasibility of a new experimental approach for shedding light on some unsolved problems on DNA elastic behavior, and this thesis represents a first step towards this direction. Understanding the DNA elasticity properties is the cornerstone for a better comprehension of its biological properties and functionalities, like DNA formation and dissociation. Nowadays three main questions are still under debate, that are the behavior of the DNA in the over-stretching regime, its elastic response at forces higher than 65 pN to 67 pN and the role played by the coupling of the stretch and twist of the molecule when it is elongated. Concerning this last aspect, the corresponding energetic contribution is proportional to the factor g, which has been recently investigated by means of molecular dynamics simulations[2] and magnetic tweezers[3, 4]. The result widely shared is that g seems to change its sign with the force, but results presented by outstanding authors contradict each others and clear and widely-accepted theoretical model explaining this effect is still lacking.

Therefore, this work presents a new experimental method based on optical-tweezers measurements, which is exploited to investigate the above mentioned issues. In particular, the motion of a bead trapped in the optical potential and linked to a single DNA molecule was investigated. A known force was applied to the system and kept constant during the measurements made with a new high-frequency data acquisition board. As a matter of fact, by looking at the force power spectrum of the bead one expects to be able to infer some informations on. The results reported represent a preliminary study which aims to a qualitative understanding of the biological system considered and sheds light on future stages of the investigation.

The first part of this work was devoted to the optimization of the experimental protocol used for getting the final results and to the preparation of optimum fluidic chambers. Concerning this last item, it is worth mentioning that the role played by the microfluidic chamber in the whole experiment is crucial. As a matter of fact, any misalignment or leaks of the channel walls as well as defects on the micro-pipette tip (often difficult to be observed to the naked eye) could negatively affect the realization of the experiments, compromising the success of a week-long measurement run. For these reasons a lot of time was spent in optimizing the preparation procedure of both the fluidic chambers and the glass micro-pipette. The home-made pipette-puller was carefully calibrated in order to obtain highly symmetric tip with a width of 2 µm, which allows avoiding undesired suction effects and uncontrolled lost of the bead during the

measurements. Moreover, a new geometry of the channel walls was designed and the final assembly of the chamber by sealing the different parts with NOA-glue was demonstrated to be the best solution, allowing to realize more resistant chambers (the mean life-time of each chamber was increased from 1 day to almost 1 week). Moreover, a new high-frequency electronic board was implemented in the optical-tweezers setup ad-hoc for this work and a detailed calibration of the acquired voltage signal was performed in the whole range of forces investigated. Concerning the force spectroscopy measurements, more than 100 molecules have been investigated and each of them were used to monitor the motion of the bead in the optical trap by applying to the system a fixed force in the range from 0 pN to 85 pN. However, it is quite difficult to carry out measurements at very high forces (above 65 pN) because the bonds between the SA beads and the DNA usually breaks. For each force power spectrum the amplitude and the corner frequency were derived by means of a lorentzian fit and the results were studied as a function of the applied force. The amplitude of the power spectrum increases clearly with the length L of the polymeric chain and at lower forces, such as $F < 15$ pN, the amplitude doesn't vary significantly, confirming the results already found in another work[47]. The same constant trend seems to be present in the over-stretch region, between 65 pN to 75 pN. Contrary of expectations, in the other force ranges the amplitude growths with the force. If a stronger dependence of A on g is supposed, it would confirm the expected twist-stretching coupling effect and its force-dependence, but it would also means that the twist-stretch coupling depends on the length of the molecule considered, which is an unprecedented result.

Concerning the corner frequency, it changes with the force and with the length of the DNA chain. Being the corner frequency directly connected with the stretch-rigidity modulus S, higher corner frequencies can be interpreted as more stiff molecules and it seems to increase as the molecule length is shorten. For all the molecules the same behavior of the corner frequency curve was observed, showing a local maximum near 35 pN, exactly where a change of the g sign is expected and interpreted as a transition from the overwind to unwind behavior of the DNA when it is stretched. Moreover, after a new local minimum in the over-stretching regions, where the DNA can be easily elongated, the corner frequency apparently increases with the force also above the over-stretching, suggesting a new remarkable variation of the coupling factor g.

The obtained results show that this new experimental approach is suitable for investigating the elastic parameters of double-stranded DNA molecules with the optical tweezers technique. However, they also highlighted, for what concerns the power spectrum amplitude, that the assumptions made for simplify the data analysis are not completely satisfied in the whole force range investigated in this work, specifically between 25 pN to 50 pN and above 65 pN.

Further investigations should be performed in the low-frequency region, for example acquiring data for a longer time, where the expected dependences of the corner frequency and the amplitude from the stretch and twist modulus, and the twist-stretch coupling are more relevant. Of course, this new possible study will require also further computational efforts, in order to simultaneously take into account all the elastic parameters during the fitting of both low- and high-frequency regimes of the power spectrum. This could highlight the role of these parameters that are used in the theoretical models of DNA

elasticity. Finally, additional data shall be taken in the region above the over-stretching regime, which have never been investigated till now, in order to have a clear and detailed view of the DNA elasticity response also at higher forces.

Bibliography

[1] Felix Ritort. "Single-molecule experiments in biological physics: methods and applications". In: *Journal of Physics: Condensed Matter* 18.32 (2006), R531.

[2] Alberto Marin-Gonzalez et al. "Understanding the mechanical response of double-stranded DNA and RNA under constant stretching forces using all-atom molecular dynamics". In: *Proceedings of the National Academy of Sciences* 114.27 (2017), pp. 7049–7054.

[3] Jan Lipfert et al. "Double-stranded RNA under force and torque: Similarities to and striking differences from double-stranded DNA". In: *Proceedings of the National Academy of Sciences* 111.43 (2014), pp. 15408–15413.

[4] Jeff Gore et al. "DNA overwinds when stretched". In: *Nature* 442.7104 (2006), p. 836.

[5] Robert T Beyer. "Radiation pressure—the history of a mislabeled tensor". In: *The Journal of the Acoustical Society of America* 63.4 (1978), pp. 1025–1030.

[6] Adolfo Giuseppe Bartoli. *Sopra i movimenti prodotti dalla luce e dal calore: e sopra il radiometro di Crookes*. Coi tipi dei successori le Monnier, 1876.

[7] Ludvig Lorenz. "Sur la lumière réfléchie et réfractée par une sphère transparente". In: *Oeuvres Scientifiques* (1898), pp. 405–529.

[8] Louis Lorenz. *Lysbevægelsen i og uden for en af plane Lysbølger belyst Kugle*. na, 1890.

[9] Gustav Mie. "Contributions to the optics of turbid media, particularly of colloidal metal solutions". In: *Contributions to the optics of turbid media, particularly of colloidal metal solutions Transl. into ENGLISH from Ann. Phys.(Leipzig), v. 25, no. 3, 1908 p 377-445* (1976).

[10] Gustav Mie. "Beiträge zur Optik trüber Medien, speziell kolloidaler Metallösungen". In: *Annalen der physik* 330.3 (1908), pp. 377–445.

[11] Peter Debye. "Der lichtdruck auf kugeln von beliebigem material". In: *Annalen der physik* 335.11 (1909), pp. 57–136.

[12] G Gouesbet. "A scientific story of generalized Lorenz–Mie theories with epistemological remarks". In: *Journal of Quantitative Spectroscopy and Radiative Transfer* 126 (2013), pp. 7–15.

[13] Y_ Yeh and HZ Cummins. "Localized fluid flow measurements with an He–Ne laser spectrometer". In: *Applied Physics Letters* 4.10 (1964), pp. 176–178.

[14] Gérard Gouesbet. "Optical Sizing, with Emphasis on Simultaneous Measurements of Velocities and Sizes of Particles Embedded in Flows. A Plenary Lecture". In: *ICHMT DIGITAL LIBRARY ONLINE*. Begel House Inc. 1985.

[15] Gérard Gouesbet. "Generalized Lorenz-Mie theories and mechanical effects of laser light, on the occasion of Arthur Ashkin's receipt of the 2018 Nobel prize in physics for his pioneering work in optical levitation and manipulation: A review". In: *Journal of Quantitative Spectroscopy and Radiative Transfer* (2019).

[16] Arthur Ashkin. "Acceleration and trapping of particles by radiation pressure". In: *Physical review letters* 24.4 (1970), p. 156.

[17] A Ashkin and JM Dziedzic. "Stability of optical levitation by radiation pressure". In: *Applied Physics Letters* 24.12 (1974), pp. 586–588.

[18] A Ashkin and JM Dziedzic. "Optical levitation in high vacuum". In: *Applied Physics Letters* 28.6 (1976), pp. 333–335.

[19] Arthur Ashkin and JM Dziedzic. "Optical levitation by radiation pressure". In: *Applied Physics Letters* 19.8 (1971), pp. 283–285.

[20] Arthur Ashkin et al. "Observation of a single-beam gradient force optical trap for dielectric particles". In: *Optics letters* 11.5 (1986), pp. 288–290.

[21] Arthur Ashkin. "Forces of a single-beam gradient laser trap on a dielectric sphere in the ray optics regime". In: *Biophysical journal* 61.2 (1992), pp. 569–582.

[22] Arthur Ashkin and James M Dziedzic. "Optical trapping and manipulation of viruses and bacteria". In: *Science* 235.4795 (1987), pp. 1517–1520.

[23] Sarhan M Musa. "Computational Nanotechnology Using Finite Difference Time Domain". In: CRC Press, 2017. Chap. 5.

[24] Josep Maria Huguet i Casades Josep Maria Huguet i Casades. "Statistical and thermodynamic properties of DNA unzipping experiments with optical tweezers". PhD thesis. Departament de Fisica Fonamental, 2006.

[25] Clara Zaccaria. "Optical mini-Tweezers: un esperimento di singola molecola". Tesi magistrale. Università degli studi di Padova, 2018.

[26] Fang-Lin Mao et al. "Calculation of axial optical forces exerted on medium-sized particles by optical trap". In: *Optics & Laser Technology* 39.1 (2007), pp. 34–39.

[27] John David Jackson. *Classical electrodynamics*. 1999.

[28] Steven B. Smith, Yujia Cui, and Carlos Bustamante. "Optical-trap force transducer that operates by direct measurement of light momentum". In: *Biophotonics, Part B*. Vol. 361. Methods in Enzymology. Academic Press, 2003. Chap. 7, pp. 134–162. DOI: https://doi.org/10.1016/S0076-6879(03)61009-8. URL: http://www.sciencedirect.com/science/article/pii/S0076687903610098.

[29] Carlos J Bustamante and Steven B Smith. *Optical beam translation device and method utilizing a pivoting optical fiber*. US Patent 7,274,451. Sept. 2007.

[30] Carlos J Bustamante and Steven B Smith. *Light-force sensor and method for measuring axial optical-trap forces from changes in light momentum along an optic axis*. US Patent 7,133,132. Nov. 2006.

[31] Keir C Neuman and Steven M Block. "Optical trapping". In: *Review of scientific instruments* 75.9 (2004), pp. 2787–2809.

[32] Norio Yagi et al. "The role of DNase and EDTA on DNA degradation in formaldehyde fixed tissues". In: *Biotechnic & histochemistry* 71.3 (1996), pp. 123–129.

[33] URL: https://www.chemsrc.com/en/cas/1672-46-4_409065.html.

[34] URL: https://www.chemsrc.com/en/cas/58-85-5_509663.html.

[35] James D Watson, Francis HC Crick, et al. "Molecular structure of nucleic acids". In: *Nature* 171.4356 (1953), pp. 737–738.

[36] Pik-Yin Lai and Zicong Zhou. "B-to S-form transition in double-stranded DNA with basepair interactions". In: *Physica A: Statistical Mechanics and its Applications* 321.1-2 (2003), pp. 170–180.

[37] John F Marko. "Stretching must twist DNA". In: *EPL (Europhysics Letters)* 38.3 (1997), p. 183.

[38] Steven B Smith, Yujia Cui, and Carlos Bustamante. "Overstretching B-DNA: the elastic response of individual double-stranded and single-stranded DNA molecules". In: *Science* 271.5250 (1996), pp. 795–799.

[39] Peter Gross et al. "Quantifying how DNA stretches, melts and changes twist under tension". In: *Nature Physics* 7.9 (2011), p. 731.

[40] L Bongini, V Lombardi, and P Bianco. "The transition mechanism of DNA overstretching: a microscopic view using molecular dynamics". In: *Journal of The Royal Society Interface* 11.97 (2014), p. 20140399.

[41] Hauke Clausen-Schaumann et al. "Mechanical Stability of Single DNA Molecules". In: *Biophysical Journal* 78.4 (2000), pp. 1997–2007. ISSN: 0006-3495. DOI: https://doi.org/10.1016/S0006-3495(00)76747-6. URL: http://www.sciencedirect.com/science/article/pii/S0006349500767476.

[42] Carlos Bustamante et al. "Entropic elasticity of lambda-phage DNA". In: *SCIENCE-NEW YORK THEN WASHINGTON-* (1994), pp. 1599–1599.

[43] John F Marko and Eric D Siggia. "Stretching dna". In: *Macromolecules* 28.26 (1995), pp. 8759–8770.

[44] C. Bouchiat et al. "Estimating the Persistence Length of a Worm-Like Chain Molecule from Force-Extension Measurements". In: *Biophysical Journal* 76.1 (1999), pp. 409–413. ISSN: 0006-3495. DOI: https://doi.org/10.1016/S0006-3495(99)77207-3. URL: http://www.sciencedirect.com/science/article/pii/S0006349599772073.

[45] Randall D Kamien et al. "Direct determination of DNA twist-stretch coupling". In: *EPL (Europhysics Letters)* 38.3 (1997), p. 237.

[46] Baiesi M. and Seno F. "Power spectrum of DNA stretching". Interna report. 2019.

[47] Timothée Lionnet et al. "Wringing out DNA". In: *Physical Review Letters* 96.17 (2006), p. 178102.

[48] Andrew Marantan and L Mahadevan. "Mechanics and statistics of the worm-like chain". In: *American Journal of Physics* 86.2 (2018), pp. 86–94.

[49] *DAQ 6023E/6024E/6025E User manual*. National Instruments Corporation.

[50] Arthur Ashkin. "History of optical trapping and manipulation of small-neutral particle, atoms, and molecules". In: *IEEE Journal of Selected Topics in Quantum Electronics* 6.6 (2000), pp. 841–856.

[51] Craig F Bohren and Donald R Huffman. *Absorption and scattering of light by small particles*. John Wiley & Sons, 2008.

[52] William H Press et al. *Numerical recipes*. Cambridge university press Cambridge, 1989.

[53] Kirstine Berg-Sørensen and Henrik Flyvbjerg. "Power spectrum analysis for optical tweezers". In: *Review of Scientific Instruments* 75.3 (2004), pp. 594–612.

[54] A Buosciolo, G Pesce, and A Sasso. "New calibration method for position detector for simultaneous measurements of force constants and local viscosity in optical tweezers". In: *Optics communications* 230.4-6 (2004), pp. 357–368.